

# Towards a Pointing Model for GMRT antennas - Part II

N. G. Kantharia, V. K. Kulkarni, R. Nityananda

*National Centre for Radio Astrophysics,  
Tata Institute of Fundamental Research,  
Pune*

(start: May 2007) (submission: Feb 2009)

## 1 Abstract

In this technical report, we present the pointing model for GMRT antennas determined using data at 1280 MHz. Pointing offsets along the elevation axis are found to vary by  $4' - 6'$  and along the azimuth axis by  $2' - 3'$  for most antennas during a rise-to-set scan on a strong point source. The typical rms error on pointing of most antennas without the pointing model is  $\sigma = \sqrt{(\sigma_E^2 + \sigma_A^2)} \geq 2'$ . For a few antennas the change is recorded to be  $15' - 20'$  during the scan. This behaviour is repeatable at 1280 MHz and is also observed at 610 MHz. A pointing model based on the model given by Greve et al. (1996) and Ulich (1981) both of which use the derivation of Stumpf (1971) is determined from the observed GMRT data and applied to the data. The results show that the systematic elevation-dependent variation in the pointing offsets is well-accounted for by the model leaving behind residuals with rms  $\sigma = \sqrt{(\sigma_E^2 + \sigma_A^2)} \leq 1'$  which is the limitation dictated by the servo system of the GMRT antennas. In particular, the antennas which show a large variation in the elevation pointing offsets are well corrected by the model. Many antennas show a jump at 0h HA followed by hysteresis wherein the elevation pointing offsets during the rising phase and setting phase of the source are different. The model fails to correct for this degeneracy. We note here that the 0h HA jump has been known to and solved by the GMRT engineers and hence needs to be corrected mechanically. In many cases, this jump dominates the final rms on the variation in pointing offsets. We end by showing that gravitational deformation appears to be the major factor responsible for the elevation-dependent variation observed in the elevation pointing offsets whereas the errors introduced by the varying zero offset of the azimuth encoder and inclination of the elevation axis dominate the variation in the azimuth pointing offsets. The pointing model, obtained from data taken in October 2006, is able to correct the elevation pointing offsets variation to some extent, but appears to fail to correct the variation in the azimuth pointing offsets one year later. This appears to suggest that the gravitational bending term varies over a longer timescale as compared to the terms responsible for the azimuth offset variation.

## 2 Introduction

The model was based on the work by Ulich (1981), Greve et al. (1996) and Stumpf (1972) which derives a model based on the mechanical structure of an alt-azimuth mounted telescope.

We conducted our experiments in the L band where antennas have the narrowest primary beam and hence the fractional pointing offsets are largest. The L band at GMRT is divided into four sub-bands: we used the subband centred at 1280 MHz which is the most sensitive of the four. Moreover, we note that the variation of the pointing offsets in course of observing a source will result in the severest dynamic range limitation at L band. Procedures in ONLINE (GOPNTG) and programmes in C were developed where necessary to aid source selection and subsequent data acquisition. Moreover codes were developed to analyse this data and obtain a model from it. Lastly we developed an algorithm to implement the online correction of pointing offsets based on the pointing model. In the following sections, we elaborate on the above.

## 3 Experiments for a pointing model at 1280 MHz

As noted above all our experiments were conducted in the 1280 MHz sub-band. We decided to use grid pointing for obtaining the data required to estimate a pointing model. In this method, one or two antennas are used as reference antennas which continuously track the source whereas the rest of the antennas are made to observe a one dimensional grid of points along the elevation and azimuth directions. The correlations of the antennas with the reference antennas then give the primary beamshape of the antennas. By fitting gaussians to this beam, the pointing offsets are estimated. No gain calibration is effected. Thus at any given time, assuming all 30 GMRT antennas are working; the pointing model can be obtained only for 28 or 29 antennas using this method. Another round of observations with a different set of reference antennas is then required to estimate the model for the reference antennas of the first round. The alternate method involved scanning across the source and estimating the pointing offset from the difference between the expected peak time for the scan and the actual peak time. We did not want to use this method since the scope for mistakes was larger. Moreover there have been some complaints regarding the scanning method (Private communication: Subhashis Roy). To avoid complicating the model by doubts resulting from the scanning method, we used the grid pointing method.

We divided the experiment into four parts:

**Step 1.** First was to demonstrate that all the antennas consistently showed a systematic variation in pointing offsets with elevation and azimuth. Although earlier experiments had indicated the presence of such a variation, which made us propose for a pointing model, the repeatability of these results was not evident.

**Step 2.** Determine pointing offsets as a function of elevation and azimuth of the source by making observations of a large number of points in the (elevation,

azimuth) space. Then use these to obtain a pointing model for each GMRT antenna using the form of pointing model used on mm-wave antennas.

**Step 3.** Implement the pointing model for online correction of the pointing offsets during observations. Once implemented, this should result in a better dynamic range especially for the higher frequencies and probably for the lower frequencies if strong sources happened to be located near or beyond the half power points of the primary beam.

**Step 4.** Imaging data at all frequency bands in two states: with pointing model corrections and without pointing model corrections for two reasons: a) to examine the goodness of the model b) to quantify the increase in dynamic range due to the model. Preferably a field in which a strong source sits at the half power point should be selected for this check.

In this report, we describe the first three items with most of the report describing Step 2; Step 4 is yet to be implemented.

To demonstrate the repeatability of the pointing offsets, we obtained data on the strong point sources, 3C48, 3C147 and 3C286. Data taken on 3C48 on 24 August 2007 are shown in Figs. 5, 41 and 7. Notice the systematic variation over and above the random component defined by the scatter in points. Such a variation was seen in all the datasets we obtained and is evident in several other datasets shown here. Thus the need for removing the systematic error component from the variation in the pointing offset was clearly demonstrated. This variation is what we aim at removing via a pointing model. We then proceeded to Step 2.

The next step was to obtain data which covers a large range in elevation and azimuth so as to be able to estimate the several coefficients of a pointing model. This required that a source list be defined. There are two ways of defining a source list so as to maximise the sampling of the (elevation, azimuth) space. In the next subsection, we describe these two and discuss the method we adopted.

**Source list at L band:** As mentioned above, there were two methods available to us to select the sources for estimating a pointing model:

**1** Observe several sources with different coordinates (right ascension and declination) so as to obtain good sky coverage as shown in Fig. 1. If all worked well this method should use less telescope time and is the method employed at many observatories.

**2** Observe a few selected strong sources from rise to set. The sources are selected such that they have different declinations so as to result in extensive coverage in the (elevation, azimuth) space (see Fig. 1). This is the method we used for most our experiments since it is the easier of the two methods so results in fewer mistakes and also avoids repeated slewing of the telescope between several sources. In future, it should be possible to use method (1) for updating the model.

The source list shown in Fig. 1 (top) was selected from the VLA (Very Large Array) calibrator list. A total of 85 calibrators which had PPPP or one S flag for all

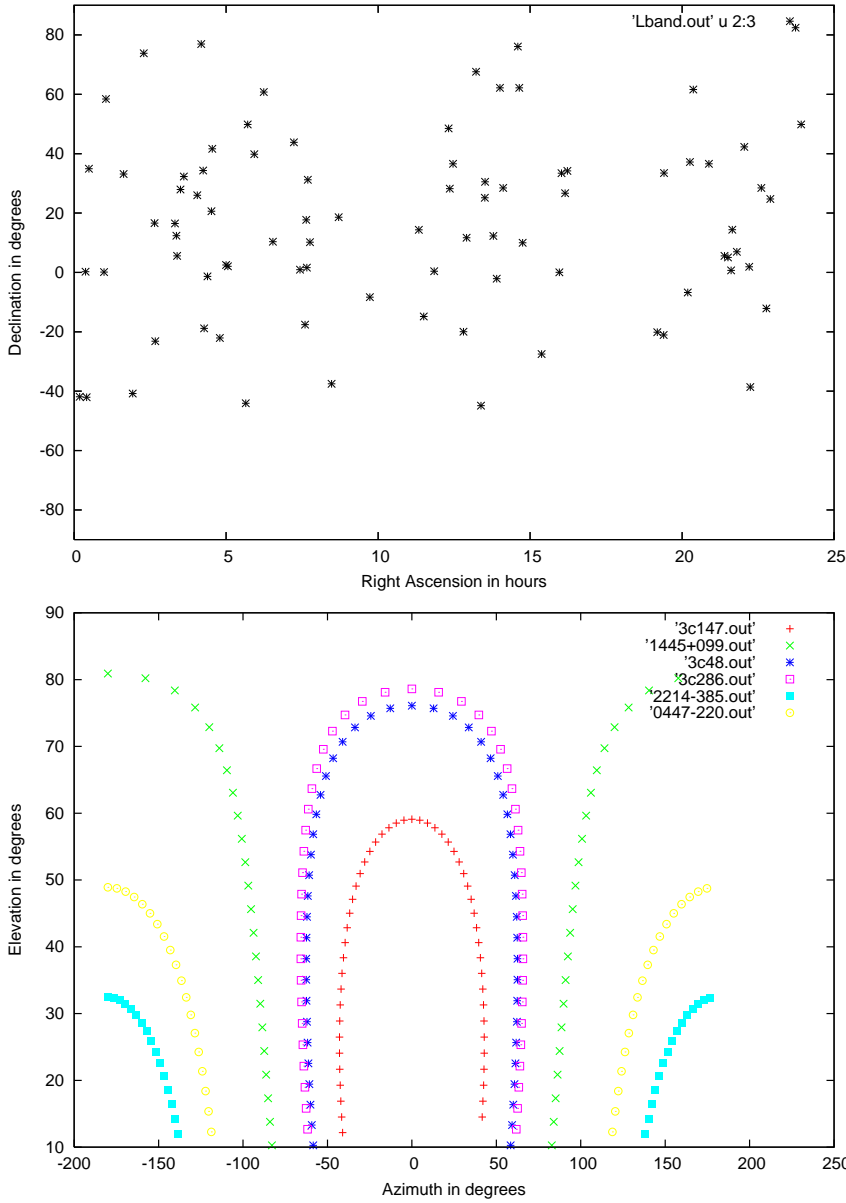


Figure 1: (top) Several sources with different  $\alpha$  and  $\delta$  can be used to obtain the model. Each point is a source. (bottom) A few sources with a range in declination can be used to obtain the model. As shown in this figure the tracks described by different sources labelled there are shown in the (elevation, azimuth) space. Notice that the coverage is good for both the methods. However method 2 would probably take longer time to complete since each source has to be followed in the sky for 8-10 hours.

the VLA arrays and strength was greater than 1 Jy at 20cm were selected. A soft copy of this list is made available with this report. Although we used the method of characterising pointing from a rise-to-set run on a single source, we developed a couple of programmes which can be used to ease the subsequent procedure of selecting sources when the model is updated by observing a large number of sources i.e method 1 outlined above. The first programme written in C (named *src*) reads in the calibrator list from a file named *Lband.list* (the order of columns is 1. IAU Name 2. epoch 3. code 4. right ascension 5. declination; ie the first line for each source in the VLA catalogue) and which, presently, is derived manually from the VLA calibrator list. This programme generates the source list. Two output files are generated by the programme namely *Lband.out* which is the source list with the coordinates converted to degrees and *Lband\_pm.src* which is the source list in the desired format required by the GMRT control system. The file *Lband.out* can be used to plot the distribution of sources in the sky. Another C programme written in C *cmd* then selects a subset of the 85 sources within a user-selected range of coordinates and also generates the relevant command file. *cmd* needs *Lband\_pm.src* as the input file and it prompts the user for a range in right ascension and declination within which it searches for sources which can be observed. The other input it requires from the user is regarding the grid which is to be observed i.e the grid endpoints, grid size and grid step; these form the variable set for the procedure *gopntg*. This programme also generates two output files: first one is the reduced source list *Lband\_sub.src* in the desired format and the second file is the command file *Lband\_pm.cmd* which uses all the selected sources. All the output files are in ascii format. However due to problems encountered in running the command file, we eventually could not use the command file for the pointing experiment and hence plans to combine the two programmes mentioned here were also put on hold. In the next part, we explain the procedure *gopntg* which we developed to automate and ease the procedure for the pointing experiment.

**Grid pointing procedure - *gopntg*:** The method of grid pointing used by Kantharia & Rao (2002) to characterise the primary beam was used here too. This method uses uncalibrated cross-correlation data and hence from any given observation, the pointing behaviour can be modelled for a maximum of 29 antennas, since at least one antenna is used as the reference antenna. In this method, a one dimensional grid of points is observed along the elevation to determine the pointing offsets along the elevation axis and a similar grid is observed along the azimuth axis for determining the azimuth offsets (see Fig. 2). We decided to sample a region of 20' on both sides of the pointing centre with a grid spacing of 5' at 1280 MHz. Although these values are not sacred, we arrived at these considering the half power beamwidth at the L band and keeping in mind that some antennas showed either a large pointing offset variation during the course of a rise-to-set run or they showed a large jump in the pointing offset when the source crossed 0h hour angle. Thus, a grid of nine points along the elevation axis with the source position defining the reference centre and a similar 1d grid along the azimuth axis were defined. The points were offset from the source position

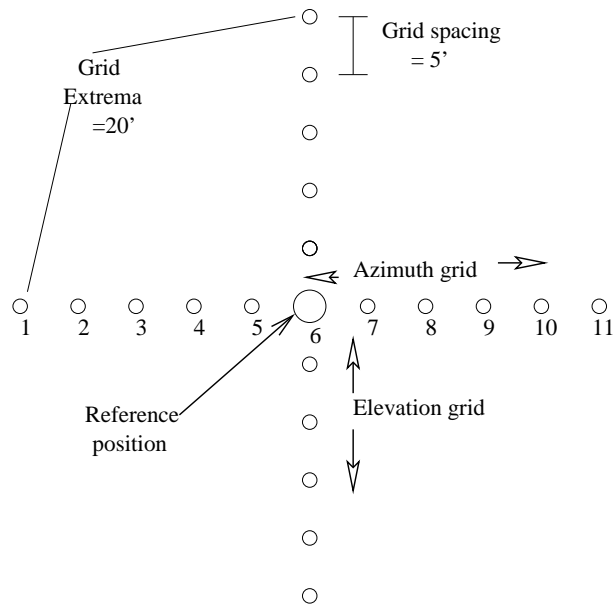


Figure 2: The grid of points observed along the elevation (vertical) and azimuth (horizontal) axes to determine the pointing offsets along the two axes at 1280 MHz. The position of the grid extrema and grid spacing are fixed depending on the observing frequency.

in steps of 5' reaching a maximum offset of 20' in either direction as shown in Fig. 2. The grid of points along the elevation axis were first observed followed by the grid of points along the azimuth axis. After observing each grid point, the source position was loaded into the antenna control system and then the offset broadcast to the antennas wrt to the source position. Thus, in practise the antennas were moved along both the elevation and azimuth axis between two grid points. The grid of points centred on the point source were continuously observed to get a good coverage of pointing offsets versus elevation and azimuth of the source.

To make the above process simpler, a procedure was developed by us in the POPS environment of the GMRT control system ONLINE. The procedure named *gopntg* was designed to help bookkeeping jobs in addition to sending commands to the antenna control system and acquiring data. The procedure names the grid point being observed by adding a character (E for elevation and A for azimuth) to the source name which specifies whether it is an elevation or azimuth grid point. It also appends the source name with a grid index which runs from 0 to 8 (or any higher number required) and which specifies the corresponding grid point (see Fig. 2). This change was kindly made in the *user5*, *suba5* environment of the ONLINE control system using the *TPARM* parameters by A. Pramesh Rao. Note that at GMRT, the convention is to attribute a positive pointing offset if the actual peak leads the expected peak and a negative offset if the actual peak lags the expected peak. See Fig. 3 for a visual version of the above

statement.

The procedure *gopntg* takes four arguments: the offset of the first point of the grid from the source position (*grdbeg*), the grid step (*grdsp*), the total number of points in an elevation/azimuth grid (*grdnopts*) and the source name (*srcname*). So the syntax of this procedure in *user5* is: *gopntg*(*grdbeg*, *grdsp*, *grdnopts*, '*srcname*'). After including the values of the arguments which we used for the 1280 MHz pointing observations, the procedure to be run for the source '3C48' would be *gopntg*(-20, 5, 9, '3C48').

The information passed to the ONLINE by the procedure is that the source name is 3C48, the first grid point (*gridbeg*) is  $-20'$  offset from the source position (ie at a lower elevation in case of an elevation grid and less by  $20'$  in case of an azimuth grid), the step between the grid points is  $5'$  and the total number of grid points is 9. Thus the grid will run from  $-20'$  to  $+20'$  in steps of  $5'$ . For each run of the procedure, first the elevation grid is observed which is followed by the azimuth grid. While the step in the grid is constant for all elevation grids, the stepsize required along the azimuth axis depends on the elevation of the source for the azimuth grid i.e. it should be  $\text{grdsp}/\cos(\text{elevation})$  to maintain a stepsize of *grdsp* at all elevations. As is obvious, the servo step is larger at high elevations and close to *grdsp* at low elevations. This information has to be sent to the servo, else it will step by *grdsp* which will result in undersampling the beam along azimuth axis at high elevations. This was also implemented in *gopntg*. The source name generated will be 3C48 - E0, 3C48 - E1, ..., 3C48 - E8 for elevation grid and 3C48 - A0, 3C48 - A1, ..., 3C48 - A8 for the azimuth grid. Within the procedure, the integration time per data point is fixed at 1 minute. Thus a total of nine elevation grid points and nine azimuth grid points adds upto 18 minutes of data and including overheads, each run of the procedure takes about 30 minutes of time. We find that we cannot further reduce the overhead time.

Note that by changing the arguments passed to *gopntg*, the source, the start point of the grid, the step and total number of points in the grid can be changed. This is required when using it to implement grid pointing at other wavebands. Below we give the recommended values of the various arguments for the different GMRT wavebands:  
*gopntg*(-40, 10, 9, '3C48') - 610 MHz  
*gopntg*(-80, 20, 9, '3C48') - 325 MHz  
*gopntg*(-120, 30, 9, '3C48') - 240 MHz  
*gopntg*(-160, 40, 9, '3C48') - 150 MHz

**Obtaining pointing data** As shown in Fig. 1b, we selected six sources which result in a good coverage in the (elevation, azimuth) space when tracked from rise to set. The selected sources were 0542+498 (3C147), 1445+099, 0137+331 (3C48), 1331+305 (3C286), 2214-385, 0447-220. The other criteria for selecting the sources listed above was to be able to follow them from rise to set and also ensure that dead time between sources was minimal. Telescope time was granted for the pointing tests and the same were scheduled in a contiguous run from saturday, 7 October 2006 4am IST to Monday, 9 October 2006 10am IST before the telescope was downed for the biannual month-long maintenance. In practise, due to some system problems we encountered during the long

observing run, we could observe only four sources namely - 3C286, 3C48, 1445+099 and 2214-385. The procedure *gopntg* was run on these sources so as to obtain the relevant pointing data. Although the easiest would be to include an infinite loop within the procedure or within a command file which runs the procedure, we found that due to a bug we were unable to abort the procedure midway without corrupting the entire control system. This meant that one had to wait for a *gopntg* run to be completed before the control system handed back the control to the user via the command line. Moreover, another bug prevented us from running the procedure within a command file environment. Thus since a loop would carry on indefinitely with no scope for aborting it midway and the command file option did not work, we were forced to manually run *gopntg* every half an hour. Since there are plans to upgrade the present control system at GMRT, we did not deem it optimal use of our time to debug the above. Instead we took extensive help of our telescope operators who made sure that the procedure was run every half an hour except when a change in the source was imminent. As can be seen in Fig. 1b, observing four sources also results in good sampling in the (elevation, azimuth) plane and our results which we describe in the following sections also demonstrate that the data was sufficient to obtain the first pointing model for GMRT antennas which when applied to the antennas would reduce the rms pointing error.

## 4 Results from pointing experiment at 1280 MHz

Here, we present results of the experiments described in the previous section.

**Offsets determined from Grid Pointing:** As described in the previous section, pointing data is obtained by retaining two antennas out of the total 30 GMRT antennas as reference antennas in a separate subarray (we used subarray 4) and having them continuously track the source (labelled ‘reference centre’ in Fig. 2). The rest of the antennas are shifted to another subarray (subarray 5) and made to follow the grid along elevation and azimuth. In the procedure, the elevation grid is observed first followed by the azimuth grid. The procedure is repeated resulting in alternate elevation and azimuth pointing error data. These data which are recorded in the GMRT data format (lta) are then analysed using offline programmes developed by one of us (VKK). The data is obtained as a function of time; each scan corresponds to one grid point in Fig. 2. Since the stepsize in the grid is known, the time axis ie x-axis is trivially converted into offset in arcmins. In our experiments, the first grid point is displaced from the source coordinates by  $-20'$  and the last grid point is offset by  $+20'$ . Data from several channels are scalar averaged and the one minute data obtained for each grid point is also averaged; both resulting in improved signal-to-noise ratio. The voltage data (recall that the reference antenna continuously tracks the source whereas the other antenna involved in the cross-correlation product tracks the grid resulting in a voltage output) is also squared to convert into power units. The above is achieved by running our perl

script *pxget*. After receiving input from the user, the script *pxget* runs the programme *xtract* (author: Sanjay Bhatnagar). All the visibility data with the specified reference antenna from the raw data file (lta file) are extracted and the 1 min data obtained on each grid point are averaged to obtain one data point for each grid point. The next programme run by *pxget* is *pxcolchs* which averages frequency channels. Both these steps are focussed at improving the S/N of the data. The next programme which is run is a C programme named *pfitoff* which fits a gaussian or a higher order polynomial to the primary beam and obtains the pointing offsets along the elevation or azimuth depending on the grid of points.

The elevation and azimuth beams output by *pxget* for eight of the antennas for both polarizations are shown in Figs. 3 and 4. The data shown in these plots was obtained on 24 August 2006. The data points are shown by the filled circles, x-axis shows the grid points and is labelled in offset from the reference point, y-axis shows the amplitude and is in arbitrary units. The solid line shows the Gaussian fit to the data. The displacement between the peak of this gaussian and the zero on the x-axis gives the pointing error for that antenna and is listed in the right hand top corner in each panel. Such plots for all the antennas (excepting the reference antennas) are obtained for each run of *gopntg* and result in the pointing error data of the antennas for a given source position. This is the first step in the analysis of the pointing data.

The last programme in this suite is *plotcurv* which plots the elevation/azimuth offsets as a function of azimuth/elevation/hour angle for further analysis. Each run of *gopntg* generates one offset data point. Several such runs are conducted and all the offset data points are plotted using *plotcurv*. **azimodfit and elemodfit**. In the following we describe the results on the elevation and azimuth pointing offsets.

**Elevation pointing offsets:** Figs. 5, 41, 7 show the elevation pointing offsets plotted as a function of hour angle of the source in hours, elevation of the source in degrees and azimuth of the source in degrees respectively. As is evident from Figs. 41 and 7, there is a systematic variation in the elevation pointing offset with hour angle and elevation. The figures show data on 3C48 observed on 24 August 2006. The pointing offsets estimated from other days' data were also examined as a function of the hour angle, elevation and azimuth of the source and a similar behaviour observed. The data obtained between 7 and 9 October 2006 on four sources widely separated in declinations as shown in Fig. 1b are plotted in Fig. 8. The elevation pointing offsets as a function of the source elevation for eight antennas are shown in Fig.8. Note the similarity between Fig. 8 and Fig. 41. Note that Fig. 8 shows the variation in the elevation pointing offsets displayed by four sources.

Notice that antenna C01 shows a variation ranging from  $-10'$  to  $+10'$  in the elevation pointing offset for an elevation range of  $18^\circ$  to  $80^\circ$ . Also notice the systematic slope displayed by all the antennas and the hysteresis between the rising and setting curves for the source in Figs. 41 & 8. Note that the pointing offsets which had been determined at the start of the long observing run on October 7, using zero offset pointing were retained during the experiment. This was because some of the antennas have

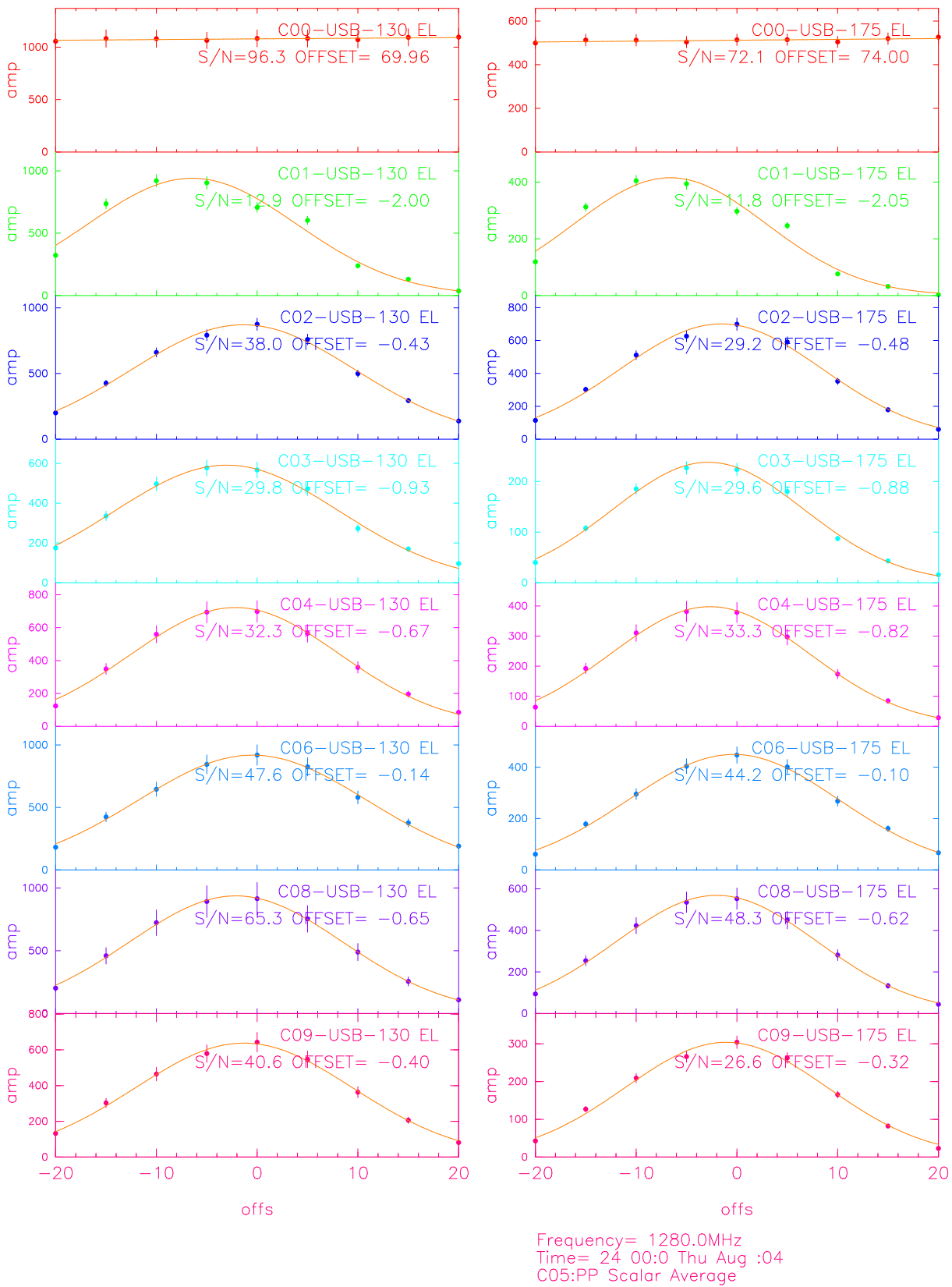


Figure 3: The pointing data for an elevation grid. Observed data are the points while the solid line is the Gaussian fit to the data. The correlations with C05 are plotted. C00 and C05 were used as the reference antennas. Note the large pointing offset in C01. The data were obtained on 24 August 2006.

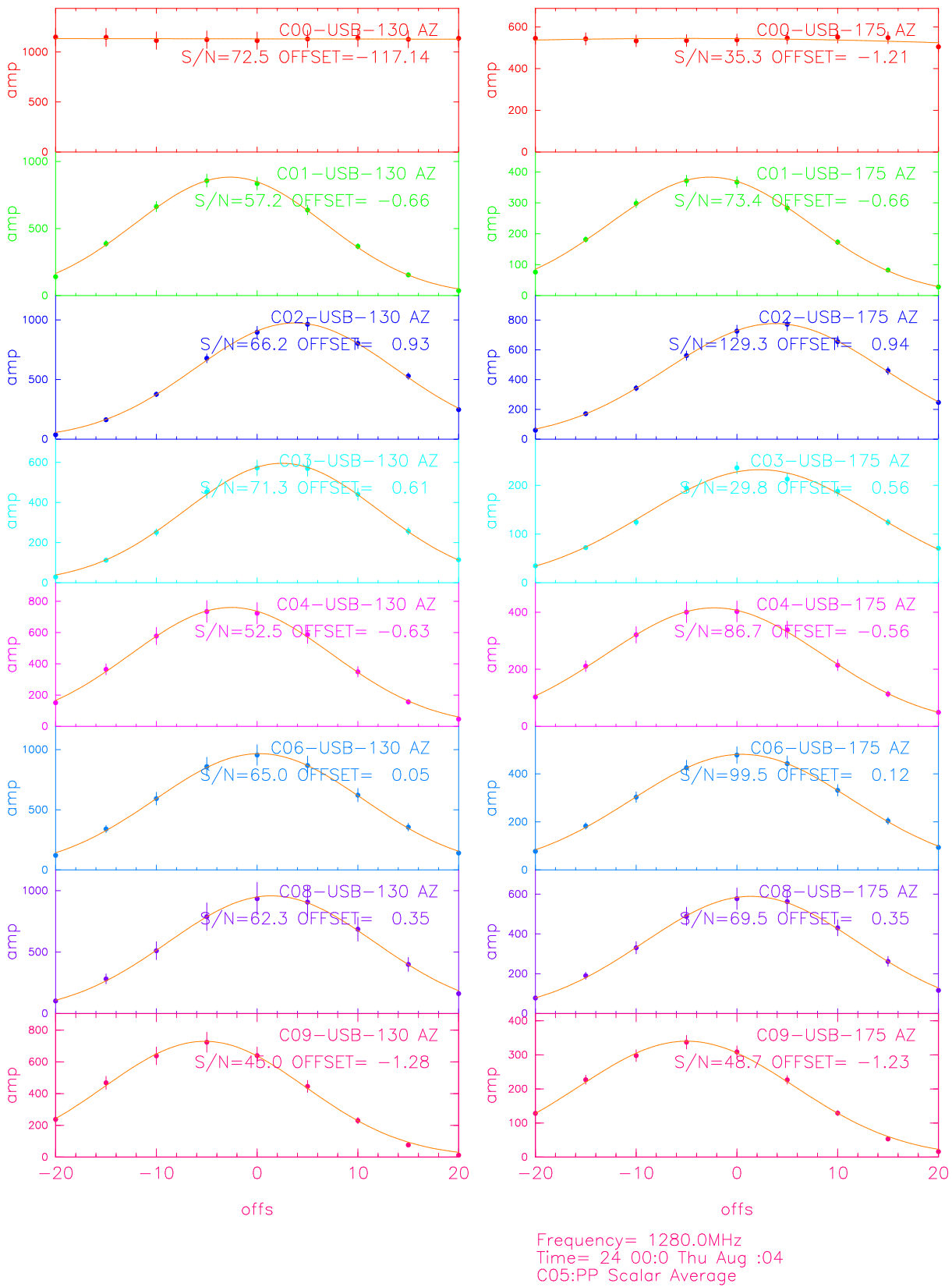


Figure 4: The pointing data for an azimuth grid. Observed data are shown by points and the solid line is the Gaussian fit to the correlation data with C05. C00 and C05 were used as the reference antennas. Note the large pointing offsets in C01 and C09. The data were obtained on 24 August 2006.

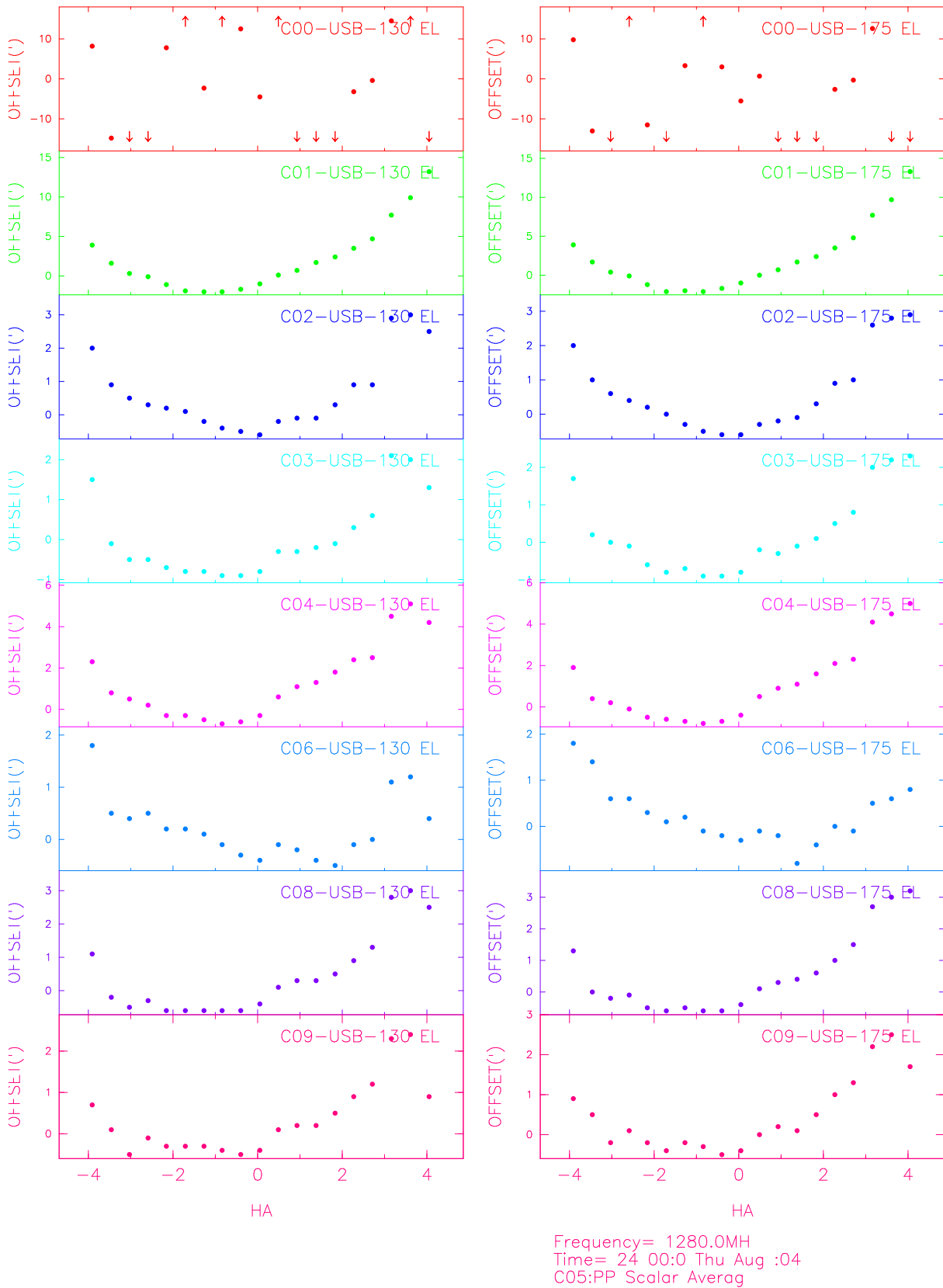
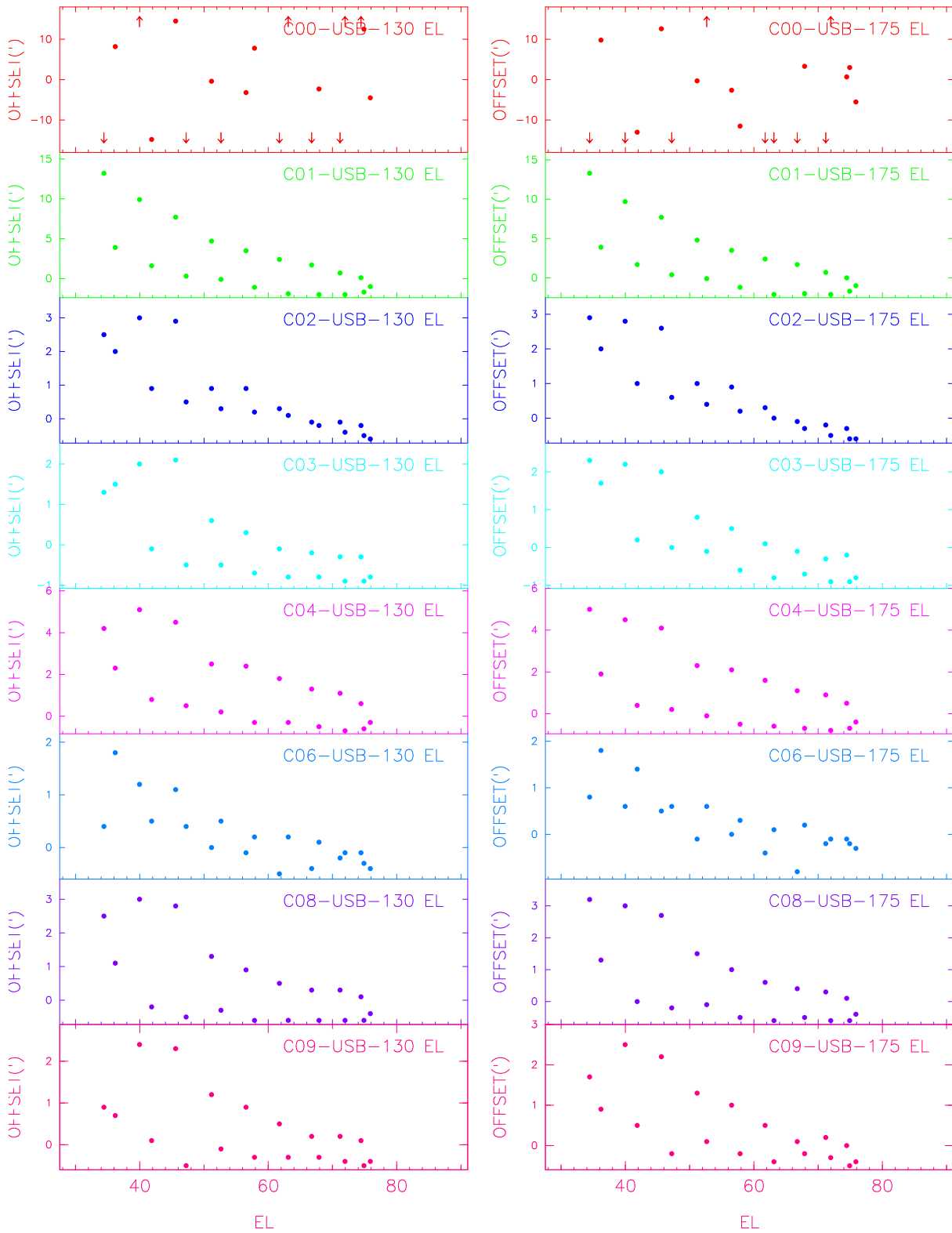


Figure 5: The elevation pointing offsets determined from several sets of data as in Fig 2 are plotted as a function of hour angle. The data were obtained on 24 August 2006. COO and C05 are the reference antennas.



Frequency= 1280.0MH  
 Time= 24 00:0 Thu Aug :04  
 C05:PP Scalar Averag

Figure 6: The elevation pointing offsets determined from several sets of data as in Fig 2 are plotted as a function of the elevation<sup>13</sup> of the source. The data were obtained on 24 August 2006. COO and C05 are the reference antennas.

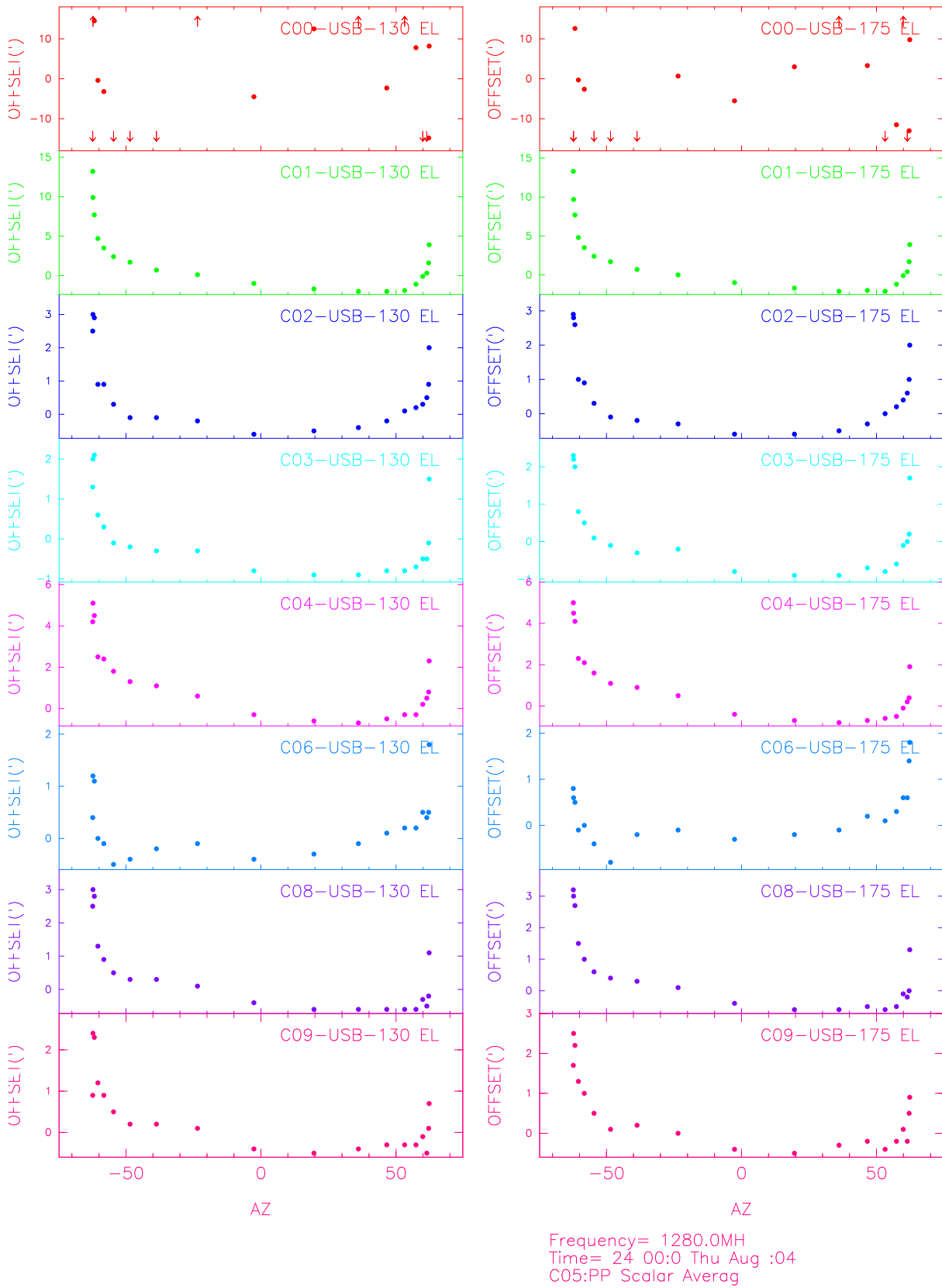
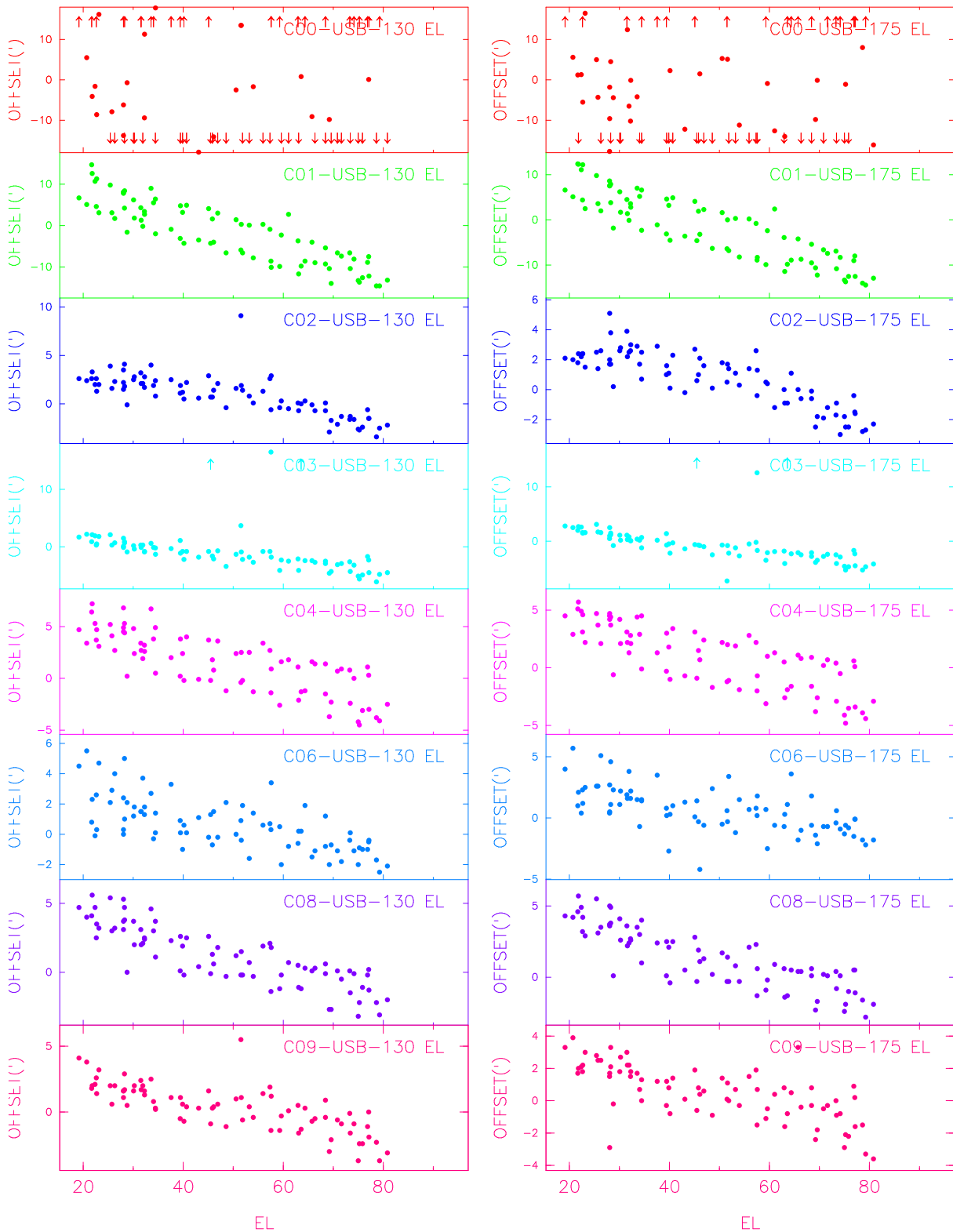


Figure 7: The elevation pointing offsets determined from several sets of data as in Fig 2 are plotted as a function of the azimuth<sup>14</sup> of the source. The data were obtained on 24 August 2006. C00 and C05 are the reference antennas.



Frequency= 1280.0MH  
 Time= Oct 7 BS= Sat 0:00  
 C05:PP Scalar Averag

Figure 8: Data from 7-9 October 2006 which was used to obtain the pointing model. Plotted here are the elevation pointing offsets as a function of elevation. C00 and C05 were used as reference antennas. There is bad point near elevation 50°.

a large ( $> 20'$ ) zero offset pointing error which if left uncorrected would either miss the source or else require a larger grid size or stepping than we have used. At GMRT, the regular pointing algorithm involves observing a very strong source such as Cas A, Cygnus A or Virgo A and scanning across the source in the ALC off mode. The self-power is then fitted by gaussians and the pointing offsets determined and uploaded to the antennas.

**Azimuth pointing offsets:** Figs. 10, 9 and 11 show how the azimuth pointing offset determined as described above varies with hour angle, elevation and azimuth of the source for eight GMRT antennas. The data were taken on the source 3C48 on 24 August 2007. Notice that the peak-to-peak variation in the azimuth pointing error is lower than that for elevation pointing errors. However there are peculiar antennas such as C02. Also note that the azimuth errors for C09 show a larger variation compared to the other antennas. Fig. 12 plots the azimuth pointing error against the source elevation for data taken between 7-9 October 2006. Notice the similarity in behaviour between Figs. 9 and Fig. 12 especially for the antennas C02 and C09.

As shown in all the above figures, both the elevation and azimuth pointing offsets are found to vary systematically as the earth rotates and the source traverses in the sky from east to west. Thus, there is a clear need to correct the erroneous pointing of the antennas using a pointing model derived from such data. We used the formulation that Ulich (1981) and Greve et al. (1996) have described and which in use on mm wave antennas. The data obtained on four sources between 7 and 9 October 2006 were used to determine a pointing model for the working antennas. We could not get a model for C00 and C05 since these were used as reference antennas. Next section discusses the pointing model.

## 5 The Pointing model

The model which we use to characterize the pointing variation of the alt-azimuth mounted GMRT antennas was taken from Greve et al. (1996). Greve et al. (1996) describe the pointing model implemented on the IRAM mm-wave telescope which is derived from the standard pointing correction model for alt-azimuth mounts based on mechanical imperfections in the antennas, originally developed by Stumpf (1972), Meeks (1968) and Ulich (1981). The functional form is presented in the Technical/Astrosupp note 'Towards a Pointing Model for GMRT Antennas - I' prepared by NGK for the pointing group. We present the model here for completion. Note that the first two terms in the model used in computing the error in the azimuth offsets are swapped in our model as compared to those given in the technical note by NGK.

The functional form of the standard pointing model for alt-azimuth mounted antennas that we use in rest of the report is taken from Greve et al. (1996) and is as follows.

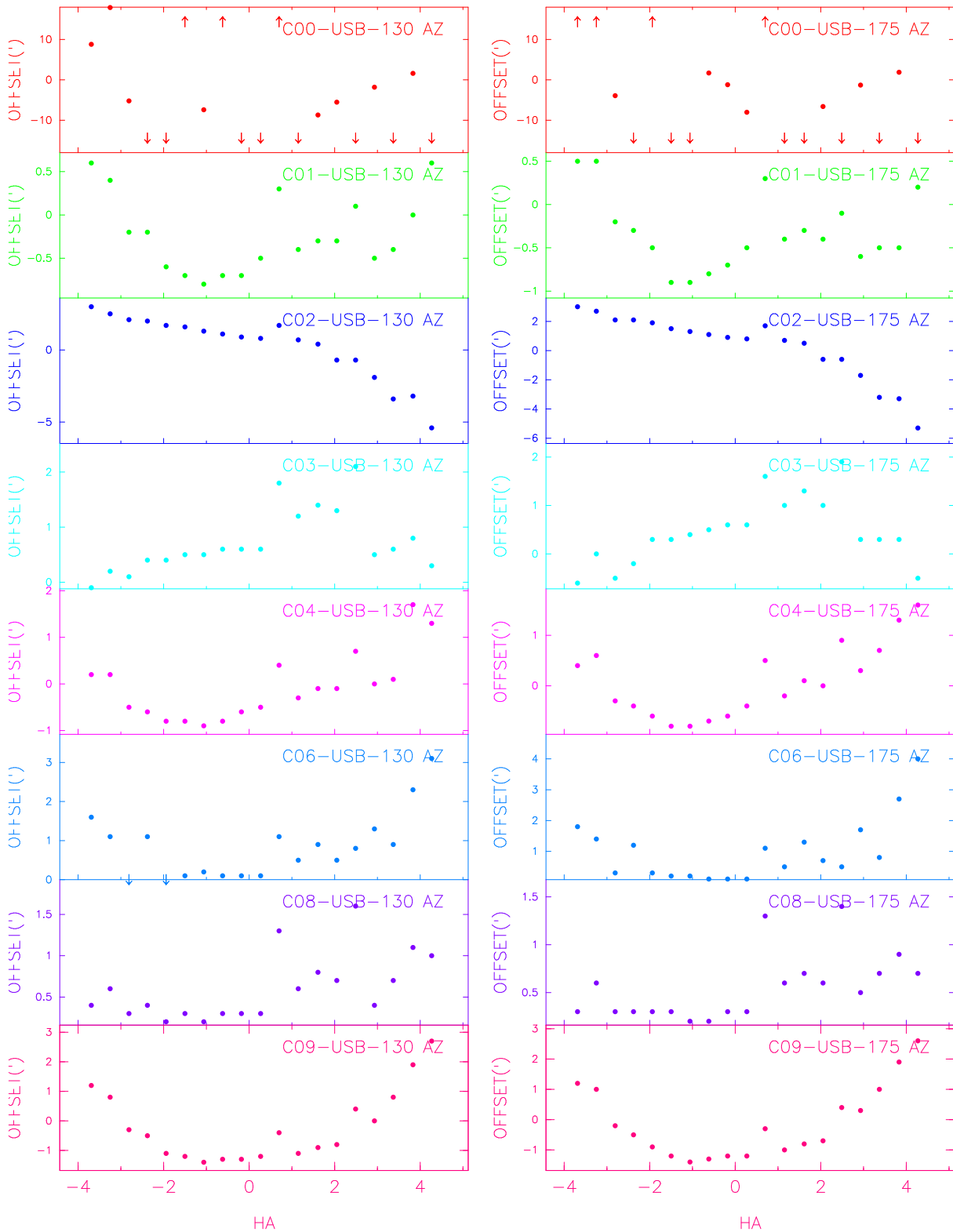
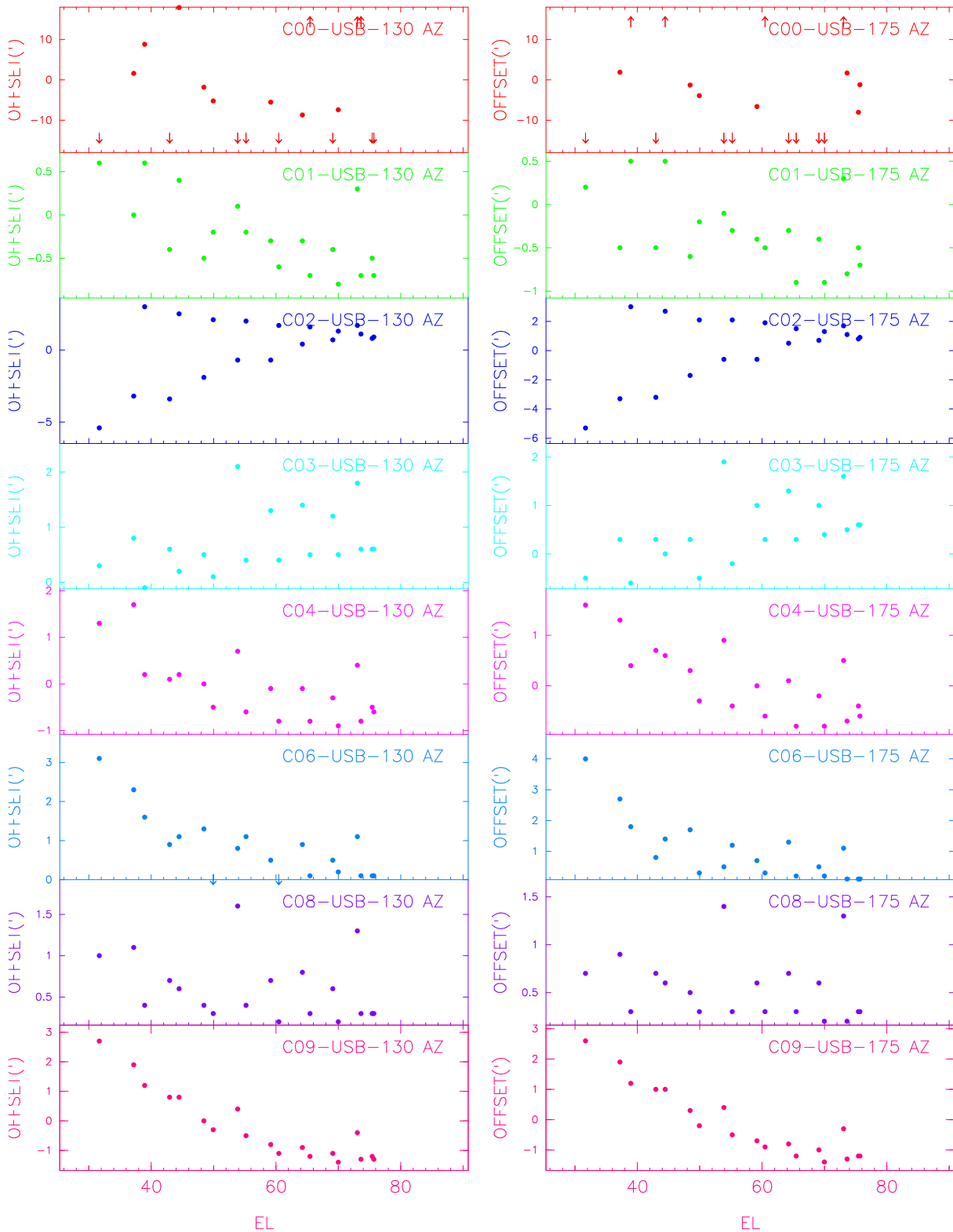
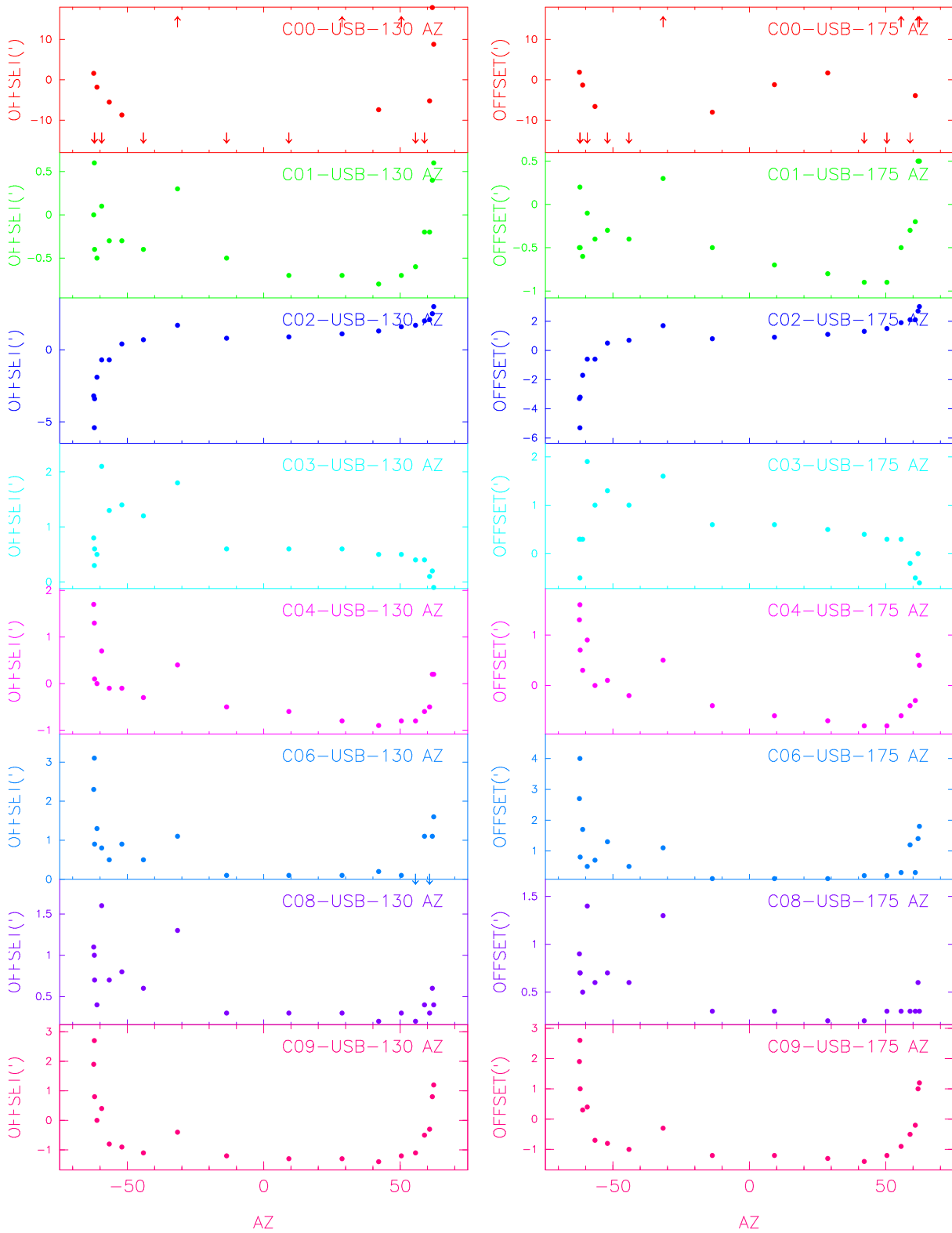


Figure 9: The azimuth pointing offsets are plotted as a function of the hour angle of the source. The data were obtained on 24 August 2006. C00 and C05 are the reference antennas.



Frequency= 1280.0MH  
 Time= 24 00:0 Thu Aug :04  
 C05:PP Scalar Averag

Figure 10: The azimuth pointing offsets determined from several sets of data as in Fig 6 are plotted as a function of the elevation of the source. The data were obtained on 24 August 2006. Notice the peculiar behaviour of C02. C00 and C05 are the reference antennas.



Frequency= 1280.0MH  
 Time= 24 00:0 Thu Aug :04  
 C05:PP Scalar Averag

Figure 11: The azimuth pointing offsets determined from several sets of data as in Fig 6 are plotted as a function of the azimuth of the source. The data were obtained on 24 August 2006. COO and C05 are the reference antennas.

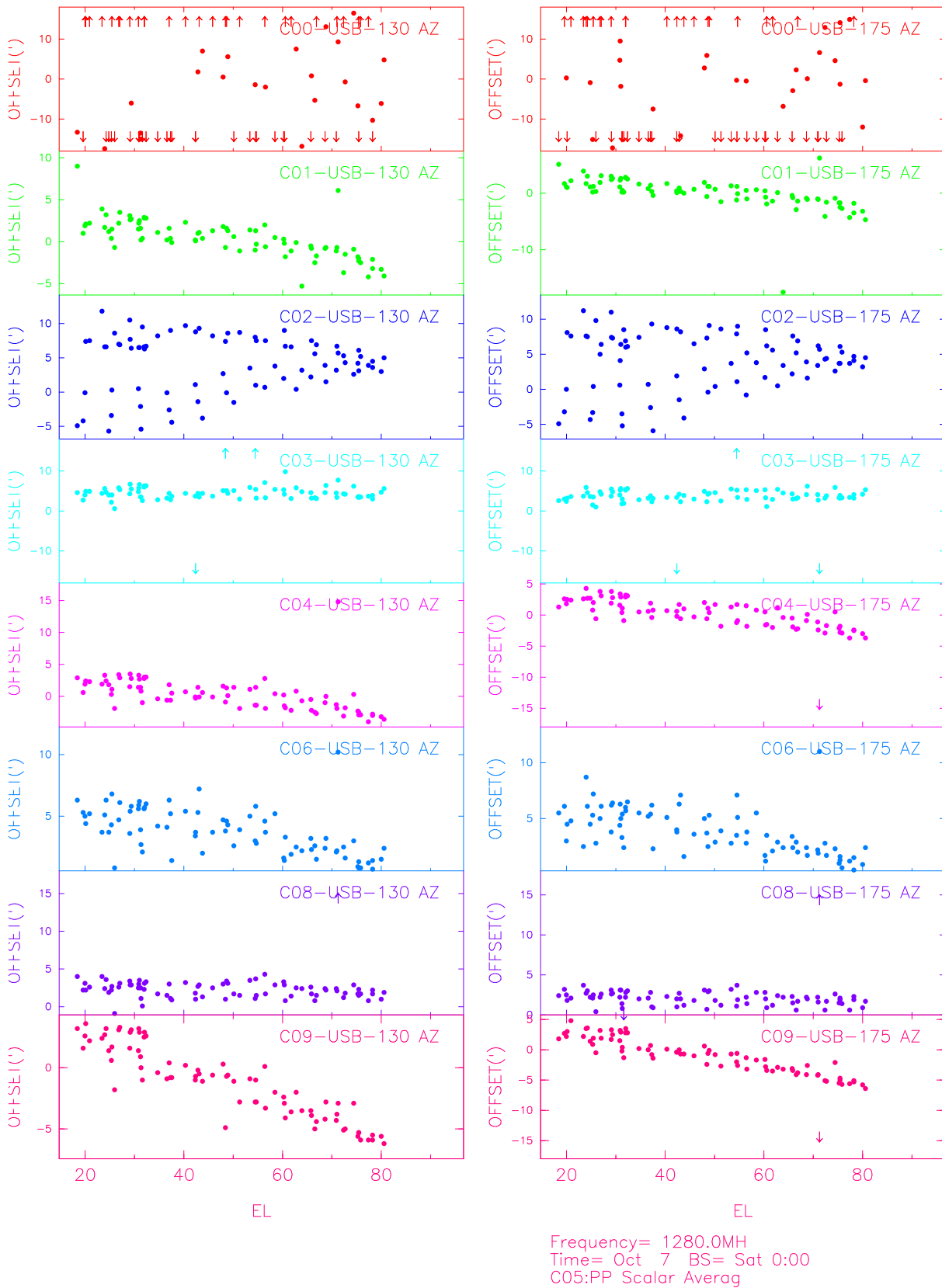


Figure 12: Data from 7-9 October 2006 which was used to obtain the pointing model. Plotted here are the azimuth pointing offsets as a function of elevation. Notice the peculiar behaviour of C02. The behaviour of the antennas is similar to that observed in the 24 August 2006 data. C00 and C05 were used as reference antennas. No correction is made to the data.

$$\Delta h = P_1 + P_2 \cos E + P_3 \sin E + P_4 \sin E \cos A + P_5 \sin A \sin E \quad (1)$$

$$\Delta v = -P_4 \sin A + P_5 \cos A + P_6 + P_7 \cos E + P_8 \sin E \quad (2)$$

$\Delta h$  and  $\Delta v$  are the corrections required in the horizontal and vertical directions to account for the pointing errors and ensure that the antennas point in the right direction. These are related to the pointing errors along the elevation ( $\delta E$ ) and azimuth ( $\delta A$ ) axes as follows:

$$\Delta v = \delta E$$

$$\Delta h = \delta A \cos(E)$$

Actual data should be fitted and the parameters  $P_i$  need to be estimated so that the values of  $\Delta v$  and  $\Delta h$  are minimized for all  $E$  and  $A$ . The parameters  $P_i$  describe the instrumental errors which result in pointing errors.  $P_1$  is the angle between the electromagnetic axis and the pointing axis (also called collimation error),  $P_2$  is the zero-offset error in the azimuth encoder,  $P_3$  is the error in the orthogonality of the elevation and azimuth axes,  $P_4$ ,  $P_5$  are errors in the azimuth axis and are the corrections required in the NS and EW directions resp,  $P_6$  is the zero-offset error in the elevation encoder and will also include an error in the feed positioning system which might occur on rotation of the turret to focus different feeds,  $P_7$  and  $P_8$  give the errors due to gravitational bending. These eight parameters are to be estimated using pointing data on sources distributed in the sky.

We note that depending on the outcome of this exercise, additional parameters can be added to the model.

**Obtaining a pointing model:** The data shown in Figs. 8, 12 obtained between 7 to 9 October 2006 were used to derive a pointing model for the GMRT antennas. We could not fit a model to C00, C05 and E04 since the first two were used as reference antennas and E04 was not working. Programmes *azimodfit*, *elemodfit* were developed to derive the coefficients  $P_i$  using the pointing errors along the elevation and azimuth axes. We initially tried fitting azimuth and elevation offsets separately but then settled for a simultaneous fit. The model described here has been obtained using a simultaneous fit to both the elevation and azimuth offsets. The programme uses the variation in the pointing errors along the elevation and azimuth axes for each antenna and estimates the best fitting model which leaves behind a random variation using the least squares technique.

**The coefficients,  $P_i$ :** The coefficients  $P_i$  in Eqn. 2 for the best fitting model are listed in Table 1. The last four lines list some nominal statistics. These coefficients are plotted in Fig. 13. From the table, it appears that the azimuth pointing errors are dominated by the coefficients  $P_2$  and  $P_3$  and the elevation pointing errors are dominated by  $P_7$  and  $P_8$ . The antenna C01 shows the largest values of  $P_7$  and  $P_8$ .

Table 1: List of coefficients of the best fit model obtained by fitting the observed variation in the elevation and azimuth pointing offsets as a function of elevation and azimuth.

Antenna	P1	P2	P3	P4	P5	P6	P7	P8
C01	-0.13	4.64	-4.07	3.29	-0.09	-1.22	14.6	-13.8
C02	2.21	0.85	2.03	0.14	2.37	0.18	5.01	-3.97
C03	2.15	1.17	1.670	0.08	-0.55	-0.69	3.76	-4.01
C04	-0.05	4.18	-3.64	1.27	-0.78	0.57	5.12	-3.66
C06	1.98	3.93	-0.89	-0.90	0.04	0.31	3.11	-2.22
C08	1.06	1.54	0.01	0.79	-0.26	0.60	4.53	-3.07
C09	-0.69	5.97	-5.96	0.16	-0.21	0.20	3.04	-2.30
C10	0.92	2.08	-0.61	1.72	-0.86	1.51	4.35	-1.78
C11	-0.01	3.15	-2.70	-0.35	-0.20	0.11	4.42	-3.56
C12	0.32	4.52	-3.46	-0.47	-0.14	0.30	3.50	-2.56
C13	0.21	3.87	-3.03	0.15	-0.22	-0.37	3.52	-3.43
C14	0.46	2.05	-1.16	0.75	-0.15	0.40	3.38	-2.35
E02	1.07	1.96	-0.30	4.05	-0.02	3.98	-1.27	6.01
E03	0.43	2.19	-1.33	-0.33	-0.92	-0.23	4.07	-3.72
E05	0.24	1.38	-0.86	1.29	0.02	0.51	5.20	-3.74
E06	1.25	0.85	0.83	0.82	-0.07	0.36	2.92	-2.02
S01	0.33	3.75	-2.78	0.18	-0.52	-0.51	7.26	-6.74
S02	0.65	3.36	-2.04	0.10	-0.33	0.57	3.29	-2.06
S03	2.40	-0.46	3.37	-1.20	-0.26	0.15	3.81	-3.01
S04	3.17	7.02	-1.88	0.85	2.72	3.99	4.47	1.09
S06	0.90	4.95	-3.10	0.51	0.43	1.16	3.89	-1.82
W01	1.22	3.81	-1.62	-0.66	2.03	0.47	1.94	-1.01
W02	0.24	2.37	-1.60	0.58	0.19	-0.79	5.91	-5.83
W03	0.68	2.06	-0.91	-0.23	-0.71	1.03	2.90	-1.17
W04	0.94	1.58	-0.17	-0.75	-0.61	0.29	2.71	-1.92
W05	1.51	0.58	1.39	0.09	-0.52	1.85	4.50	-1.50
W06	1.15	2.47	-0.71	0.53	-1.00	-0.27	2.16	-2.17
Mean	0.91	2.81	-1.24	0.46	-0.024	0.53	4.15	-2.82
RMSnoise	0.87	1.73	2.037	1.15	0.92	1.19	2.55	3.11
Median	0.90	2.37	-1.16	0.16	-0.21	0.31	3.8	-2.35
Mode	-0.13	4.64	-4.07	3.28	-0.08	-1.21	14.61	-13.8

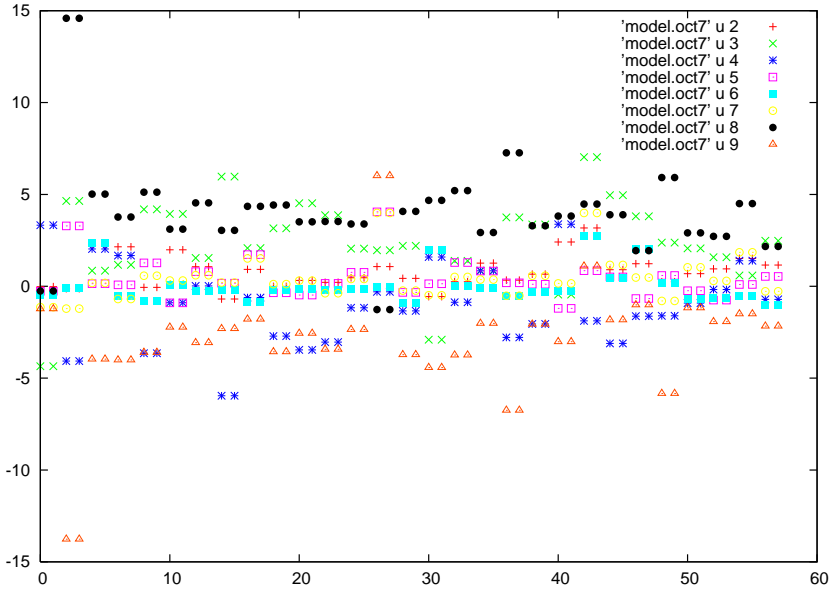


Figure 13: The coefficients of the pointing model obtained from the data taken on 7-9 October 2006. The eight coefficients of the model are listed in the top right corner. Both polarisations for a given antenna are plotted. So for example, the first two points correspond to C00 130 and C00 175 and so on. Note that the largest magnitudes are seen for the last two coefficients which correspond to gravitational deformation.

The linear model given in Section 5 were fitted to the pointing data obtained during 7 to 9 October 2006 using the least squares method and the best fit model coefficients were obtained which were then used to correct the data. The magnitude of each of the eight coefficients in minutes of arc are shown in Fig. 13 and listed in Table 1. Note that C00 and C05 were reference antennas and hence no model was found for these two antennas. Additionally E04 was not working and noisy data was obtained on W06. Hence there is no model for E04 and the model for W06 needs to be confirmed. The rest of the 26 antennas have a model derived from this data and Table 1 lists the best fit coefficients. Some inferences from these coefficients are listed below.

1. Collimation error (u2 in Fig. 13, P1 in Table 1): The coefficient appears to show some correlation with hysteresis in azimuth pointing offsets with elevation. The antennas which show large value of this coefficient: C02, C03, C06 S03, S04. Most antennas have a magnitude  $< 2'$ .
2. Zero offset Az-encoder (u3 in Fig. 13, P2 in Table 1): All working antennas except S03 have a positive value of this coefficient. The value of this coefficient ranges from 0 to  $7'$  and is one of the coefficients with the largest magnitude. The offset generated by this error will affect only the azimuth pointing and will vary as the cosine of the elevation of the source with maximum offsets at low elevations and decreasing offsets as elevation increases. Thus, this would give rise to the

variation observed in the azimuth pointing offsets with elevation especially seen for C01 and C09 (see Fig. 12) which have large coefficient values. This coefficient has no effect on the elevation pointing offset.

3. Inclusion El-axis (u4 in Fig. 13, P3 in Table 1): A large number of antennas show a negative coefficient. The value ranges from  $-6'$  to  $+3.5'$ . C01 and C09 shows the largest negative values of  $-4'$  and  $-6'$  respectively. This coefficient generates an azimuth offset which varies as  $\sin(\text{elevation})$ . It has no effect on the elevation pointing offset. The combination of this error with the previous error can easily explain the nature of the variation observed in the azimuth error with elevation of the object (see Fig.12) . This coefficient has no effect on the elevation pointing offset.
4. Inclusion Az-axis (N-S) (u5 in Fig. 13, P4 in Table 1): The magnitude of this coefficient for most antennas is  $\leq 1'$  with the range being  $-1.6'$  to  $+2'$ . The two antennas outside this range are C01 ( $3'$ ) and E02 ( $4'$ ). Recall that both show large variation in the elevation pointing offset from rise to set and also a large jump in the pointing position at 0h HA.
5. Inclusion Az-axis (E-W) (u6 in Fig. 13, P5 in Table 1): The magnitude of this coefficient for most antennas is  $\leq 1'$  with the range being  $-1'$  to  $0.5'$ . The three antennas which have a value  $> 2'$  are C02, S04, W01. In addition to a few other antennas, C01 and E02 show particularly small ( $-0.09$  and  $-0.02$  resp) values for this coefficient.
6. Zero-offset EL-encoder (u7 in Fig. 13, P6 in Table 1): This coefficient ranges from  $-1.2'$  to  $4'$  with a mean of  $0.5'$ . The antennas which have uncommonly large value of the coefficient are E02 ( $4'$ ), S04( $4'$ ) and W05 ( $2'$ ). This coefficient does not depend on the elevation or azimuth of the source and results in a constant elevation pointing error.
7. Gravitational bending (u8 in Fig. 13, P7 in Table 1) : This coefficient introduces an error in the elevation pointing offset which varies as the cosine of the elevation of the source. The mean value for this coefficient is  $\sim 4'$  and most antennas have a value between  $2'$  and  $6'$  for this coefficient. C01 shows the largest value of this coefficient ( $\sim 15'$ ).
8. Gravitational bending (u9 in Fig. 13, P8 in Table 1): This coefficient introduces an error in the elevation pointing offset which varies as the sine of the elevation of the source. The mean value for this coefficient is  $\sim -3'$ . While C01 has largest value of  $-14'$  for this coefficient, E02 ( $6'$ ), S01( $-7'$ ), W02( $-6'$ ) also have a large value of this coefficient. The error in the elevation pointing offsets which varies with elevation is dominated by the linear combination of this coefficient and the previous coefficient (C7).

In the following section, we describe the algorithms used for conducting the experiment. In the subsequent sections, we describe our results.

### **The Algorithms for obtaining a pointing model:**

*For conducting the experiments:* The 1280 MHz sub-band within the L band of GMRT was used to obtain pointing data towards several well-known radio sources. We acquired one observing run at 610 MHz to examine the variation in the pointing offsets and compare with the nature of the variation at 1280 MHz. We developed the procedure GOPNTG which runs in the POPS environment of the ONLINE control system and is described more in section 3. Moreover programmes were developed to select a set of sources which can be used for pointing and prepare a command file. The algorithm we followed for the experiments was, in brief, as follows.

- Estimate the pointing offsets on a strong radio source (e.g. M87, Cas A, Cygnus A) using the self coefficients of all the 30 antennas. These values were then loaded into the control computer.
- Select a list of sources to observe for obtaining a pointing model. These ,as explained in section 3 should be either a few strong sources which have different declinations (e.g. 3C147, 3C48... ) or it can be several sources distributed in the sky.
- Point all antennas to a source (e.g. 3C286, 3C48,...) which is bright and unresolved for GMRT. Shift two working antennas to one subarray (subarray 4 (user4) is generally used) and shift the rest of the antennas to subarray 5 (subarray 5 (user5) is the only subarray where the procedure GOPNTG has been implemented).
- Set up the data acquisition chain in user4 and user5.
- Run procedure GOPNTG in the user5 environment. GOPNTG as described earlier takes four inputs namely the starting point of the grid, the separation between the grid points in minutes of arc, the number of grid points and the source name. Each run of GOPNTG takes about 30m if using the settings described in section 3 where more details can also be found.
- After a run of GOPNTG is over, it should be run again till the end of the desired run.
- The data is written in a lta file with proper nomenclature for the sources. These data are then ready for analysis as described in the next sub-section.

## 6 Correcting antenna pointing using the model

### 6.1 Offline pointing correction

The linear pointing model derived using the data from 7-9 October 2006 was also used to correct the same data of the systematic pointing variation. The results are presented here.

**Elevation offsets:** The observed variation in the elevation pointing offsets as a function of elevation for the data taken on 7-9 October 2006 is shown in Fig. 8. These data were then offline-corrected using the derived pointing model. The corrected data are shown in Fig 20. Note the absence of the systematic variation observed in the pointing offsets as a function of elevation in the uncorrected data (Fig. 8). In the right hand top corner of each panel, the rms variation of the pointing offsets is noted. *RMSB* denotes the rms variation before the pointing model is applied and *RMSA* shows the rms variation after the pointing model is applied. For example, for antenna C01, RMSB is 7.5' whereas RMSA is 1.7'. The model has improved the rms variation by more than a factor of 4! For the rest of the antennas which do not show such a large variation in the elevation pointing offsets, there is still an improvement by a factor of two in the rms variation after the model corrections are applied to the data. To examine how effective is the model on data obtained on other days, we applied this model to data taken on 24 August 2006 (see Fig. 41). Fig. 15 shows the corrected data of 24 August 2006. On comparing RMSB and RMSA, an improvement by about a factor of two is evident in many of the antennas. Moreover comparing Fig. 15 with Fig. 8, it is evident that the model has removed the systematic variation leaving behind the hysteresis. In fact, for most antennas, the final rms variation is dominated either by the hysteresis or bad data points rather than the random scatter in the points. The corrected data is not centred on zero offset since the experiment is conducted with some pointing corrections values loaded in the encoder. This will be eventually corrected for. Note that C00 and C05 were reference antennas. Data on rest of the antennas are shown in the Appendix. We safely conclude that the model derived from October 2006 data is applicable to the data from August 2006.

In Figs. 16a,b, we show data obtained on 6 December 2006 - two months after the pointing model was estimated. Fig. 16a shows the observed variation in the pointing offsets and no model has been applied to the data. The model was then applied offline to the offsets and Fig. 16b shows the result. Comparing the two figures, it is obvious that the model has removed the systematic variation in the offsets but has failed to correct the jump observed near 0h hour angle and the hysteresis which follows. Since no terms in the present model can account for the hysteresis, it persists and dominates the final rms of the variation. However again using RMSB and RMSA as a measure of efficacy of the model, the improvement by a factor of two or more is obvious in almost all the antennas shown in Fig. 16. Thus the model is applicable after two months indicating that it characterises the antenna behaviour well.

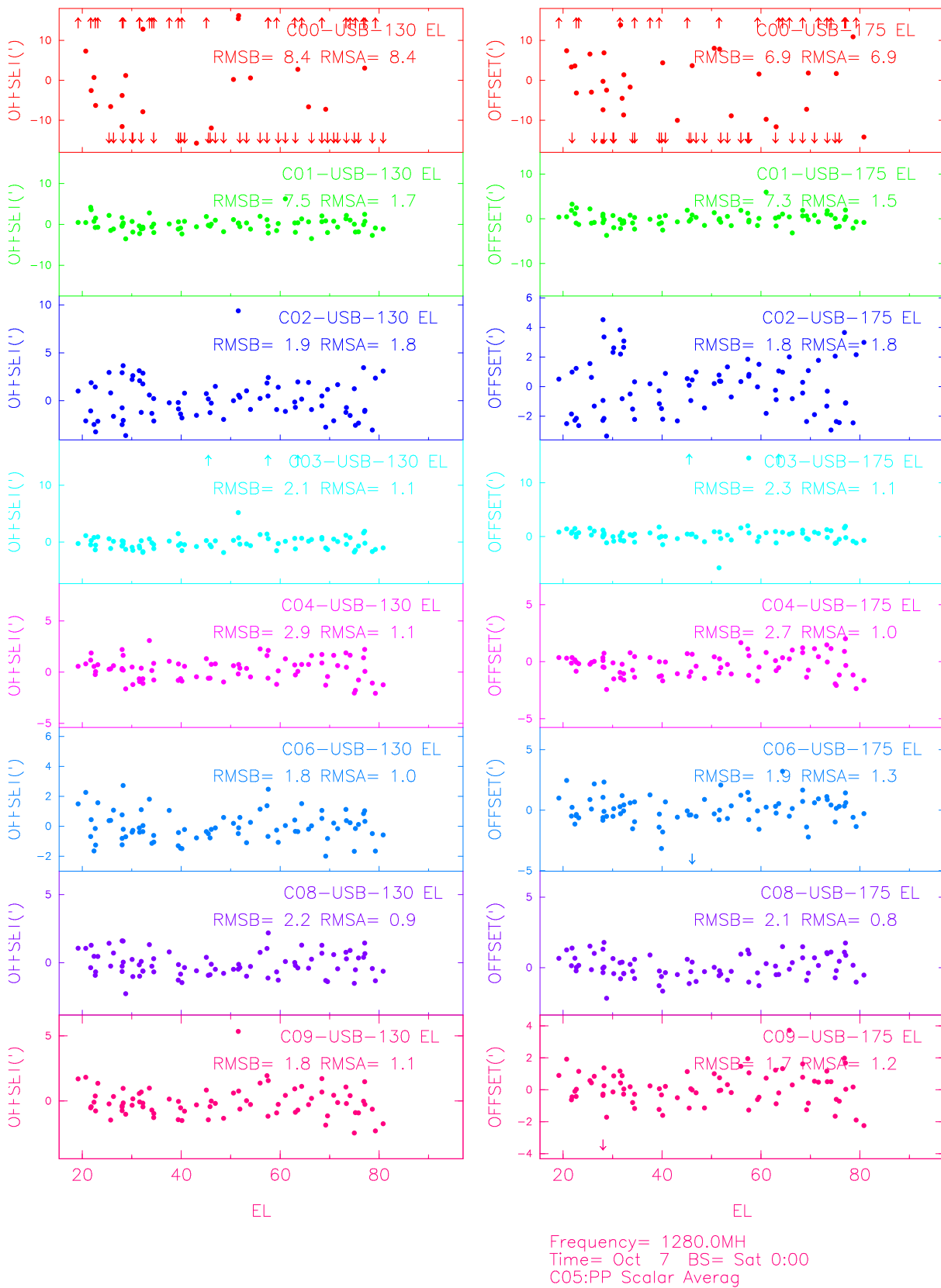


Figure 14: Data from 7-9 October 2006 after the pointing model was applied. Plotted here are the elevation pointing offsets as a function of elevation. C00 and C05 were used as reference antennas.

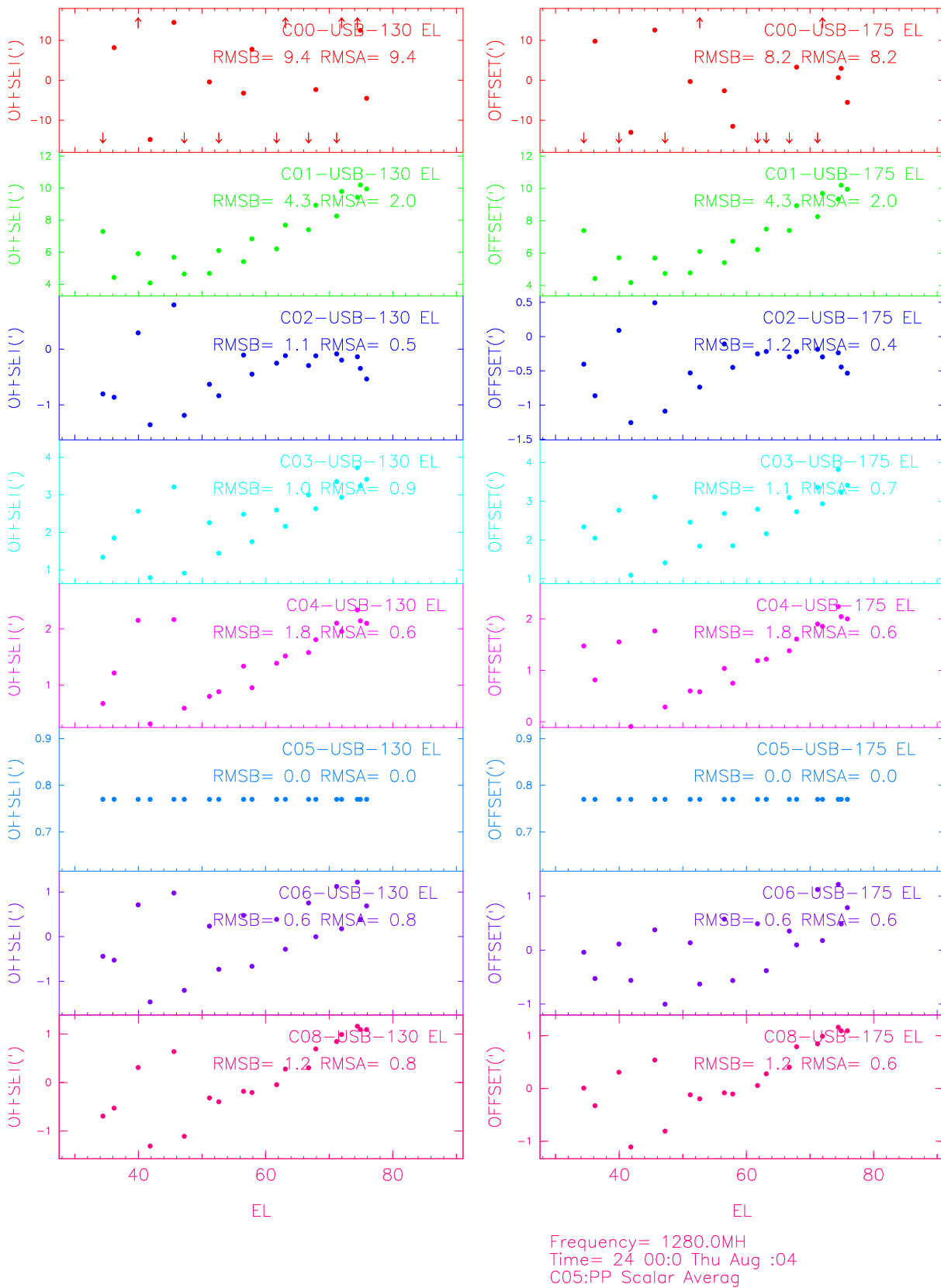


Figure 15: Data of 24 August 2006 after the pointing model was applied. Plotted here are the elevation pointing offsets as a function of elevation. C00 and C05 were used as reference antennas.

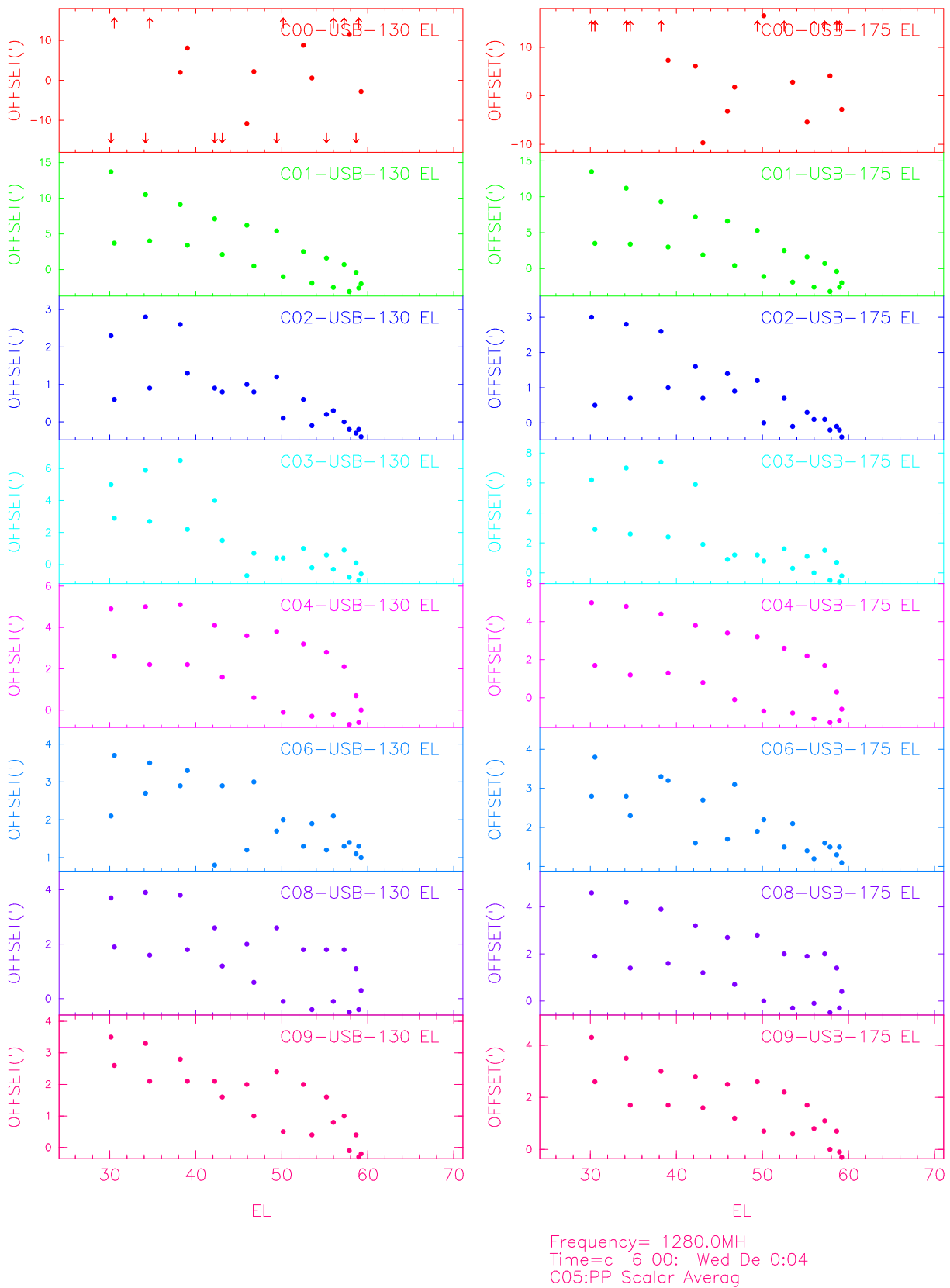


Figure 16: (a) Data of 6 December 2006 at 1280 MHz - no pointing model has been applied. Plotted here are the elevation pointing offsets as a function of elevation. Notice the systematic variation and the hysteresis.

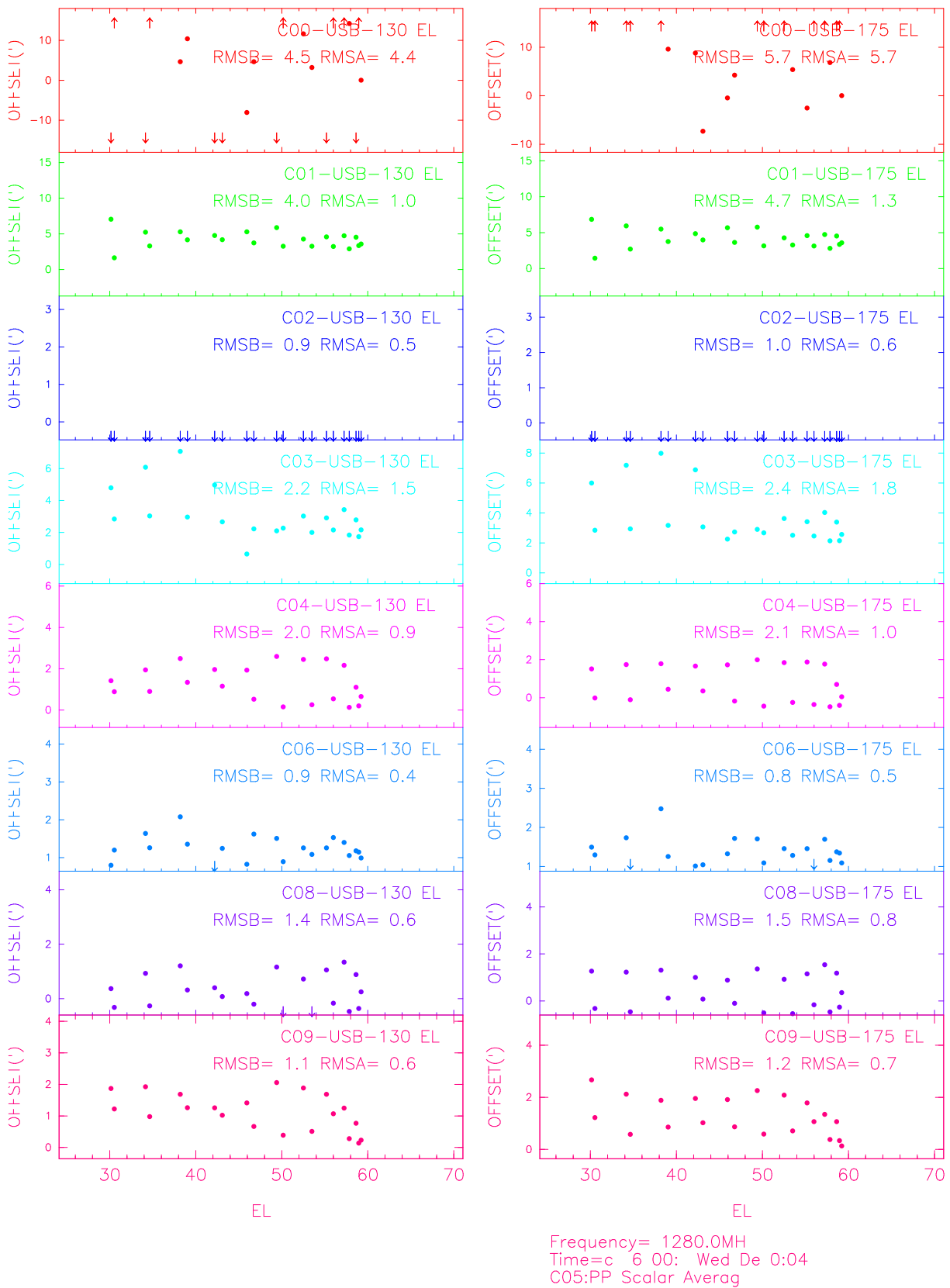


Figure 16: (b) Same data as in (a) but after offline model correction. Although the model has corrected for the monotonic variation, the hysteresis persists. Notice the RMSB and RMSA in the top right side of each panel.  $RMSA < RMSB$  in most of the cases indicating that the model has removed the systematic monotonic variation which dominates RMSA.

**Azimuth offsets:** The observed variation in the pointing offsets along the azimuth direction for the data between 7 and 9 October 2006 is shown in Fig. 12. The corrections using the pointing model were applied to this data and the results are shown in Fig. 21. Again using RMSA and RMSB as a measure of the goodness of the model, it is clear that RMSA is better than RMSB with a typical improvement by a factor  $\leq 1.5$ . The problem with C02 appears to be peculiar and is not corrected by the model with little improvement in the model-corrected offsets. We also applied this model to the data obtained on 24 August 2007 (Fig. 10). The result is shown in Fig. 18. Since the data on this day is only on one source and the RMSB is already fairly low, the difference between RMSA and RMSB is not significant as it was in the case of the elevation offsets. However it can be seen that the model either leaves the variation unchanged or there is a slight decrease in the variation after the model correction is applied to the offsets.

In Figs. 19a, b are shown the azimuth offset data from 6 December 2006. Fig. 19a shows the offsets before any model correction is applied. Fig. 19b shows the results after the corrections using the pointing model are applied to the offsets. Comparing RMSB and RMSA, we find that there is reduced variation in the offsets after correcting for the model. Thus we conclude that the model is effective after two months.

In Figs. 20, 4, the RMSB (in red) and RMSA (in green) are plotted against the antenna number for both the elevation and azimuth offsets for the data taken between 7 and 9 October 2006 and for 24 August 2006. The improvement in the data of October 2006 is clearly visible in Fig. 20. The improvement in the elevation offsets for 24 August 2006 data is visible in Fig. 20a - however the improvement in the azimuth data is miniscule.

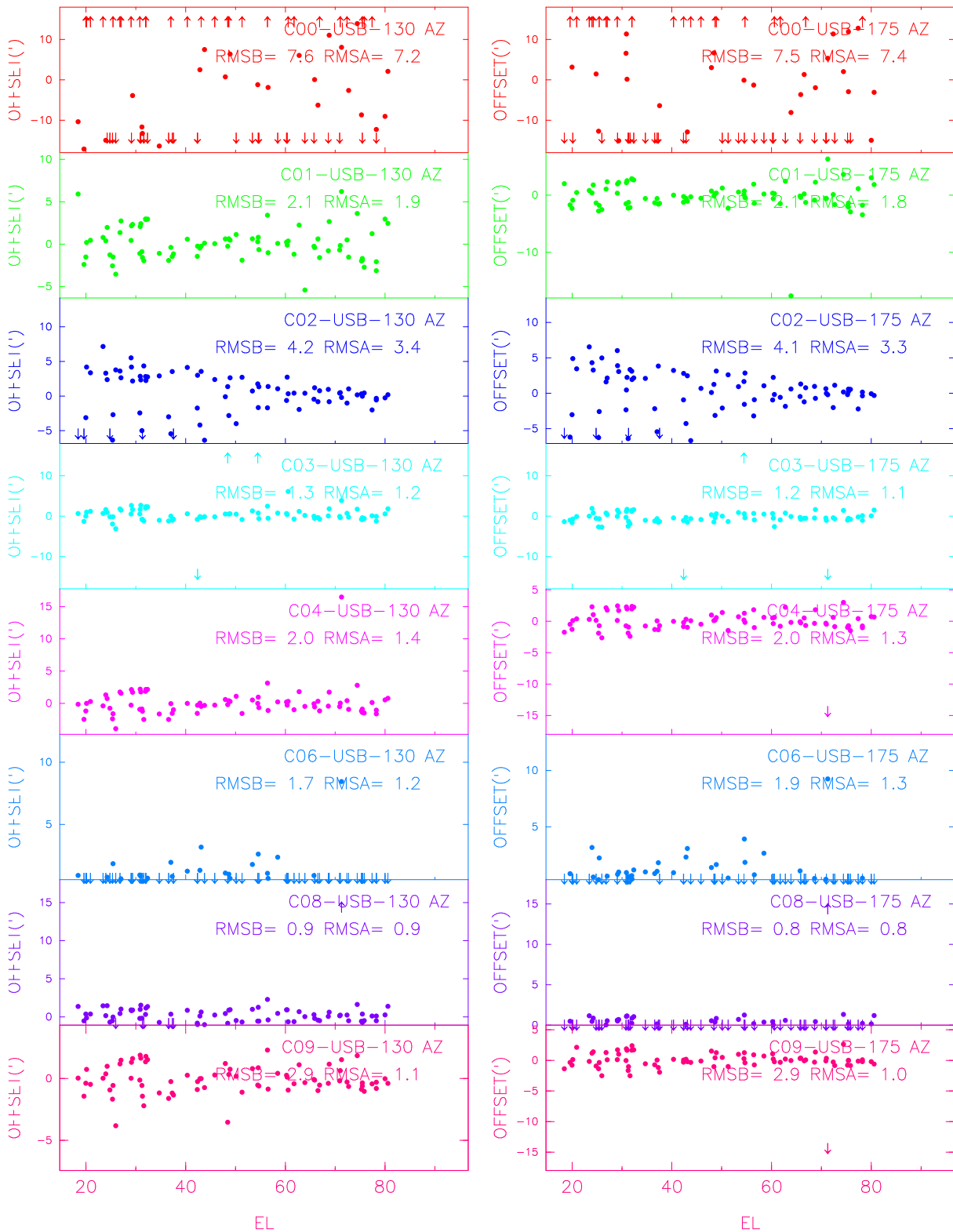
From the above discussion, it appears that the pointing model obtained from data taken between 7 and 9 October 2006 is applicable to data taken two months previous to these dates and two month subsequent to these dates. Thus the model is applicable to both the elevation and azimuth pointing offsets for at least four months.

## 6.2 Online pointing correction

### **Implementing the pointing model in the present ONLINE environment:**

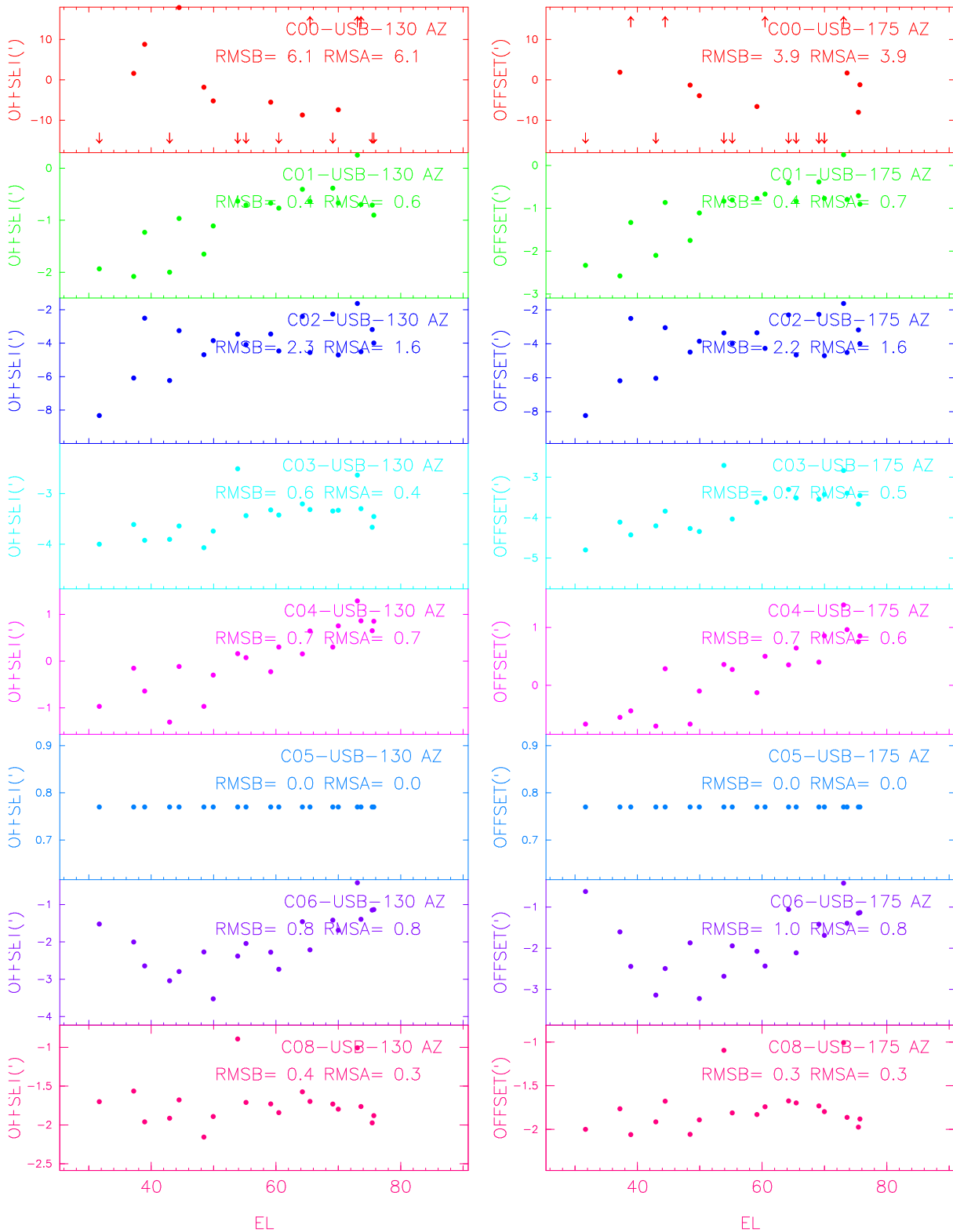
The next step after obtaining a suitable pointing model for the GMRT antennas is to implement it in the control system so that its benefits are available to GMRT users. It should be implemented in a user-friendly manner which is as invisible as possible to the end user. The present implementation is, however, not part of the control system, not is it totally invisible to the user. This scheme was dictated by two reasons : (1) ONLINE (antenna control system at GMRT) is a fairly old piece of software and hardware combination and there are plans to upgrade this. Hence it was not advisable to make major modifications to the control software (2) the end user can decide if the pointing model should be applied or not. This was required since the model is in its infancy and to begin with, we expect only some users to switch on this capability.

Thus, the present implementation of the pointing model is at the command file



Frequency= 1280.0MH  
 Time= Oct 7 BS= Sat 0:00  
 C05:PP Scalar Averag

Figure 17: Data from 7-9 October 2006 after the pointing model was applied. Plotted here are the azimuth pointing offsets as a function of elevation. C00 and C05 were used as reference antennas.



Frequency= 1280.0MH  
Time= 24 00:0 Thu Aug :04  
C05:PP Scalar Averag

Figure 18: Data of 24 August 2006 after the pointing model was applied. Plotted here are the azimuth pointing offsets as a function of elevation. C00 and C05 were used as reference antennas.

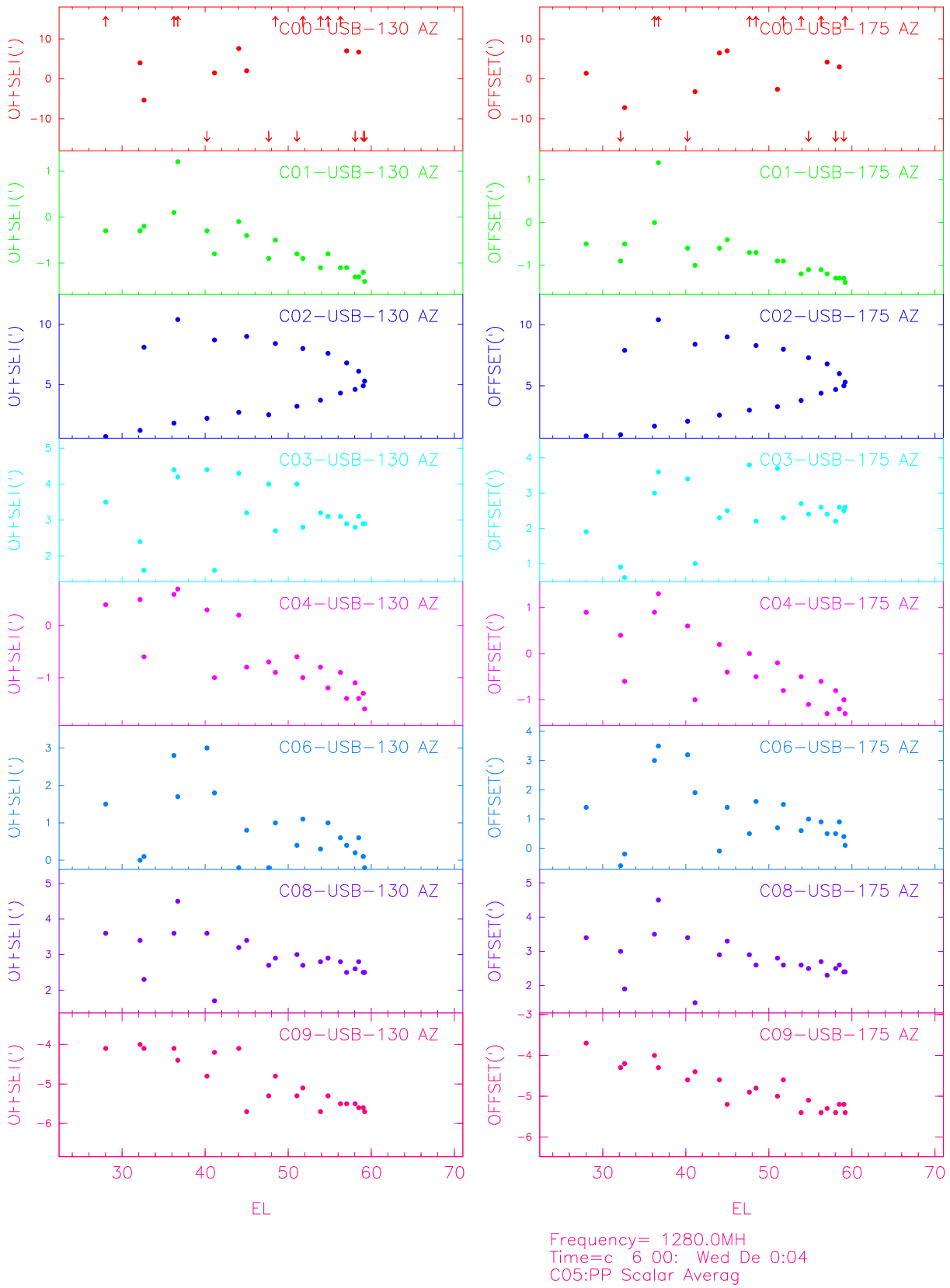


Figure 19: (a) Data of 6 December 2006 at 1280 MHz - no pointing model has been applied. Plotted here are the azimuth pointing offsets as a function of elevation.

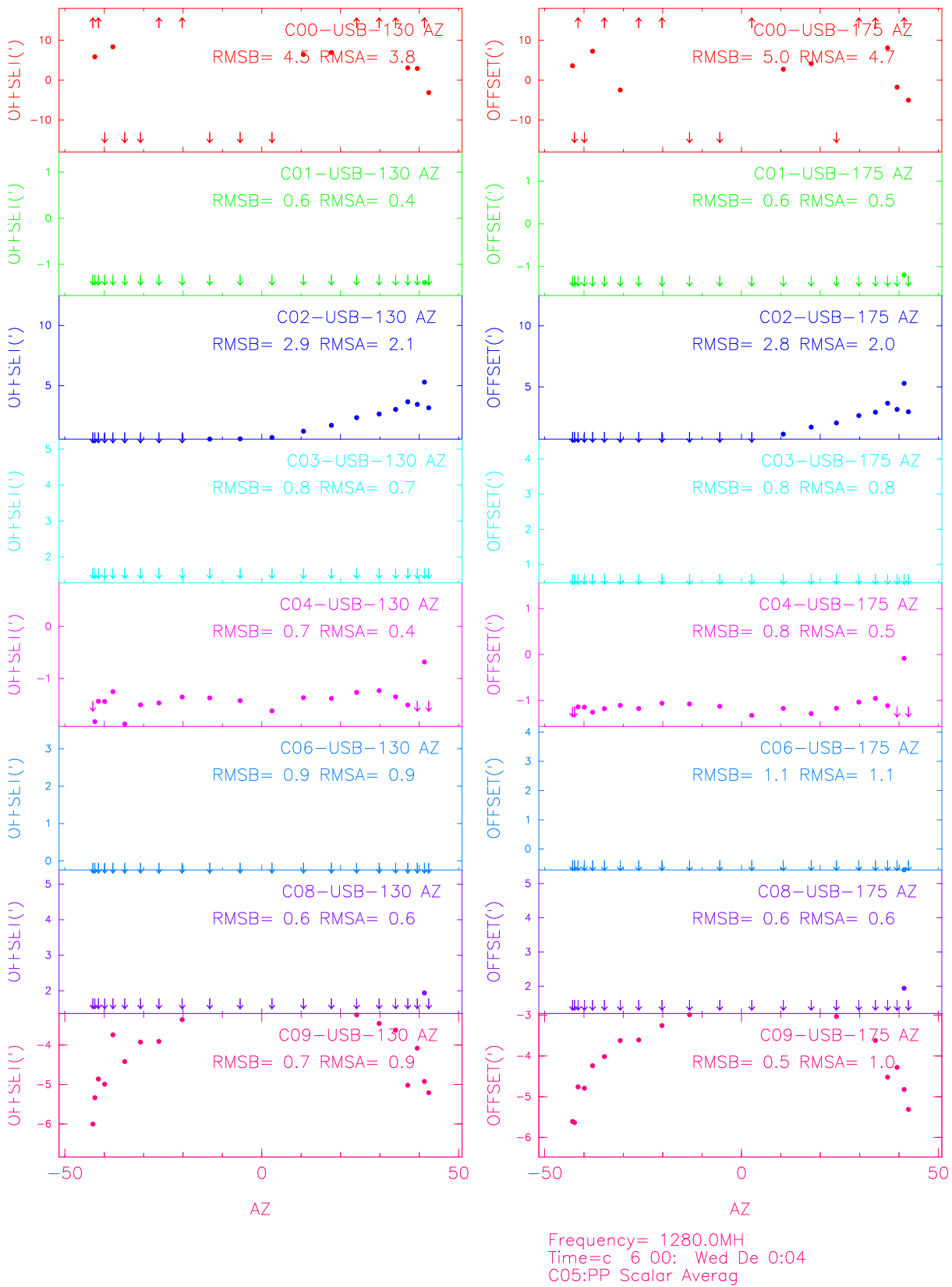


Figure 19: (b) Same data as in (a) but after offline model correction. Notice the RMSB and RMSA in the top right side of each panel.  $RMSA \leq RMSB$  in most of the cases indicating that the model has removed a systematic variation. Some of the data is not visible in the panels because of a plotting error, however RMSA and RMSB quantify the results.

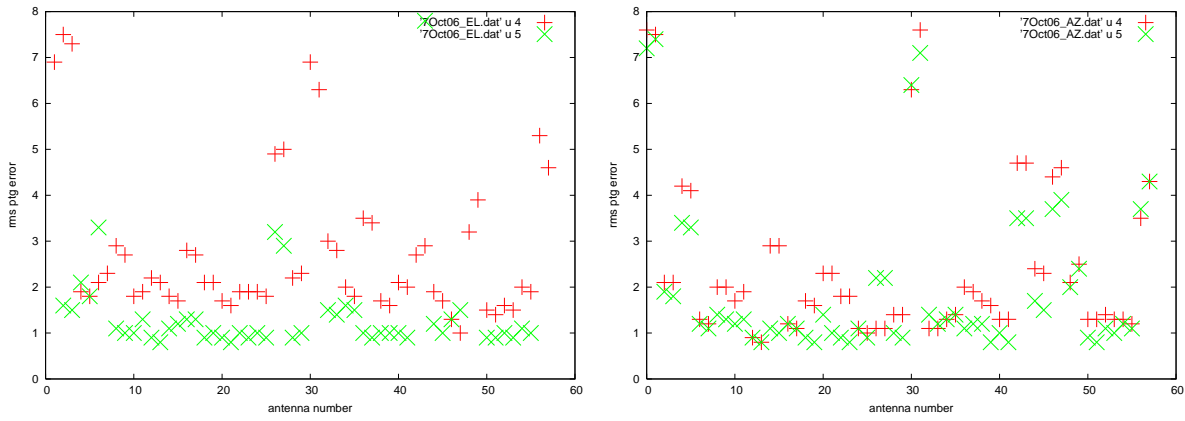


Figure 20: Data from 7-9 October 2006 after the pointing model was applied. Plotted here are the rms on the variation in pointing offsets before (red) and after (green) the model has been removed for elevation and azimuth pointing offsets.

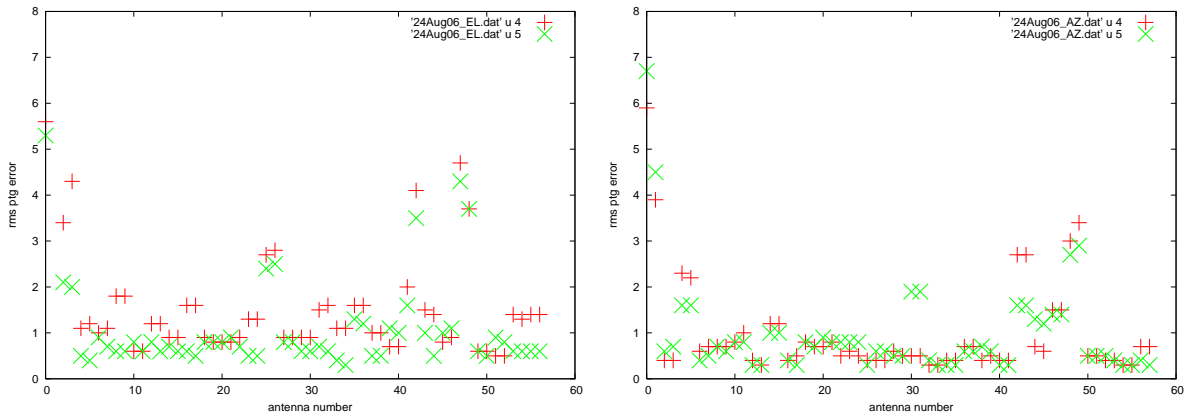


Figure 21: Data of 24 August 2006 after the model obtained from the data taken on 7-9 October 2006 was applied. Plotted here are the rms on the variation in pointing offsets before (red) and after (green) the model has been removed for elevation and azimuth pointing offsets.

level. The command file contains the set of instructions which the user gives to the GMRT control software. It includes the object names, duration of on-source time etc. All GMRT users are familiar with it. We have specified a few extra statements which when included in the command file will do the needful for an online correction of the model offsets. The lines which need to be included in the command file are:

```
/(rm /tmp/azel.dat)
/(rm /tmp/elevoff.dat)
/(rm /tmp/azimel.dat)
/(/temp2/data/deepak/wind/azel 20 > /tmp/azel.dat)
/(/export/home/astro/ngk/caloff)
/(/export/home/astro/ngk/pntg_mod_sroy.sh /temp2/data/ngk/NLDANTO.001)
/(/bell)
run ngk
```

We suggest that these lines should be inserted before the run on the phase calibrator which on the average is once every half an hour for a typical interferometric observing run. Thus, the pointing offsets will be updated using the model predictions before the phase calibrator is observed. Also this will ensure that the corrections are uploaded to the antennas every half an hour. The programmes listed here read in the present (Az, El) of the antennas (*azel*), obtain the model predictions for the offsets (*caloff*) and update the file which contains the pointing offsets for each antenna (*sroy.sh*). These are then uploaded to the antennas (*run ngk*). The command monitor has to be disabled before running these commands. Once this is done, the above procedure takes between 1 and 2 minutes to run which will have to be included as overhead time when proposing for GTAC time. However, for a typical 10-hour observing run, if the pointing corrections are done every half an hour, the overhead time would be only 38-40 minutes i.e. about 6% of the total observing time. If the command monitor is not disabled, then the above set of commands take about 20 minutes with the longest time being taken by the control system to broadcast the offsets to the antennas. This is a large overhead and cannot be tolerated. Thus, we recommend that the above commands should be run after disabling the command monitor.

### 6.3 Data obtained after online model correction

Pointing data were obtained after implementing the above algorithm. These data, if offsets were correctly applied should not show the systematic variation observed in the elevation pointing offsets. Although we encountered several problems due to bad data quality on the days we observed, we find that the online correction of the model works well for the elevation pointing offsets and the systematic variation is removed. However the same does not seem to hold for the azimuth pointing offsets.

Below we show a few datasets where model corrections were estimated and applied online to the antennas. Figs. 22, 23 show the variation in the elevation and azimuth pointing data taken on 23 January 2007 after the pointing has been corrected using the

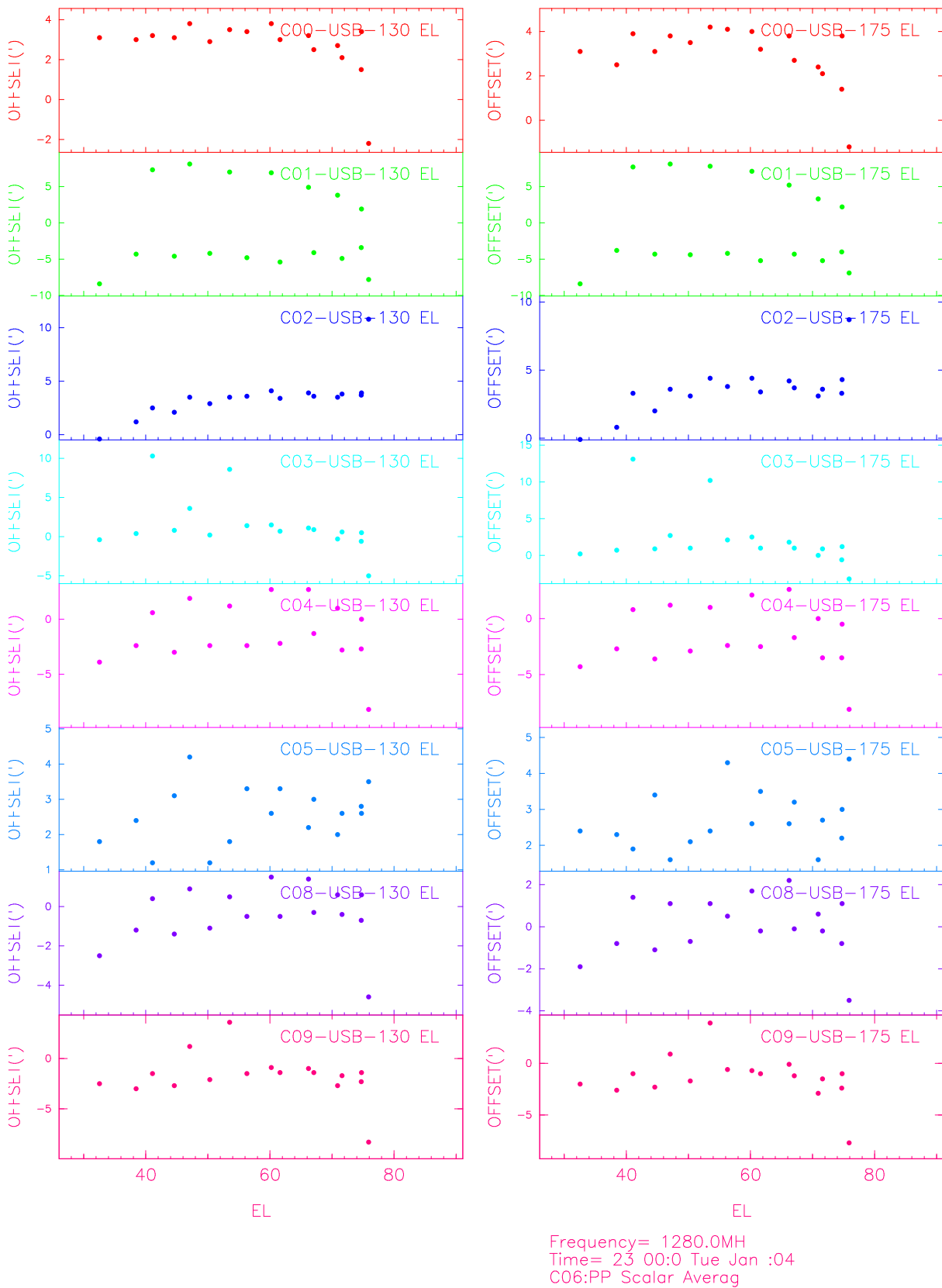


Figure 22: Online application of pointing model on data of 23 January 2007 at 1280 MHz. Plotted here are the elevation pointing offsets as a function of elevation. Note that the systematic variation has been removed but the hysteresis persists. The last data point appears to be bad.

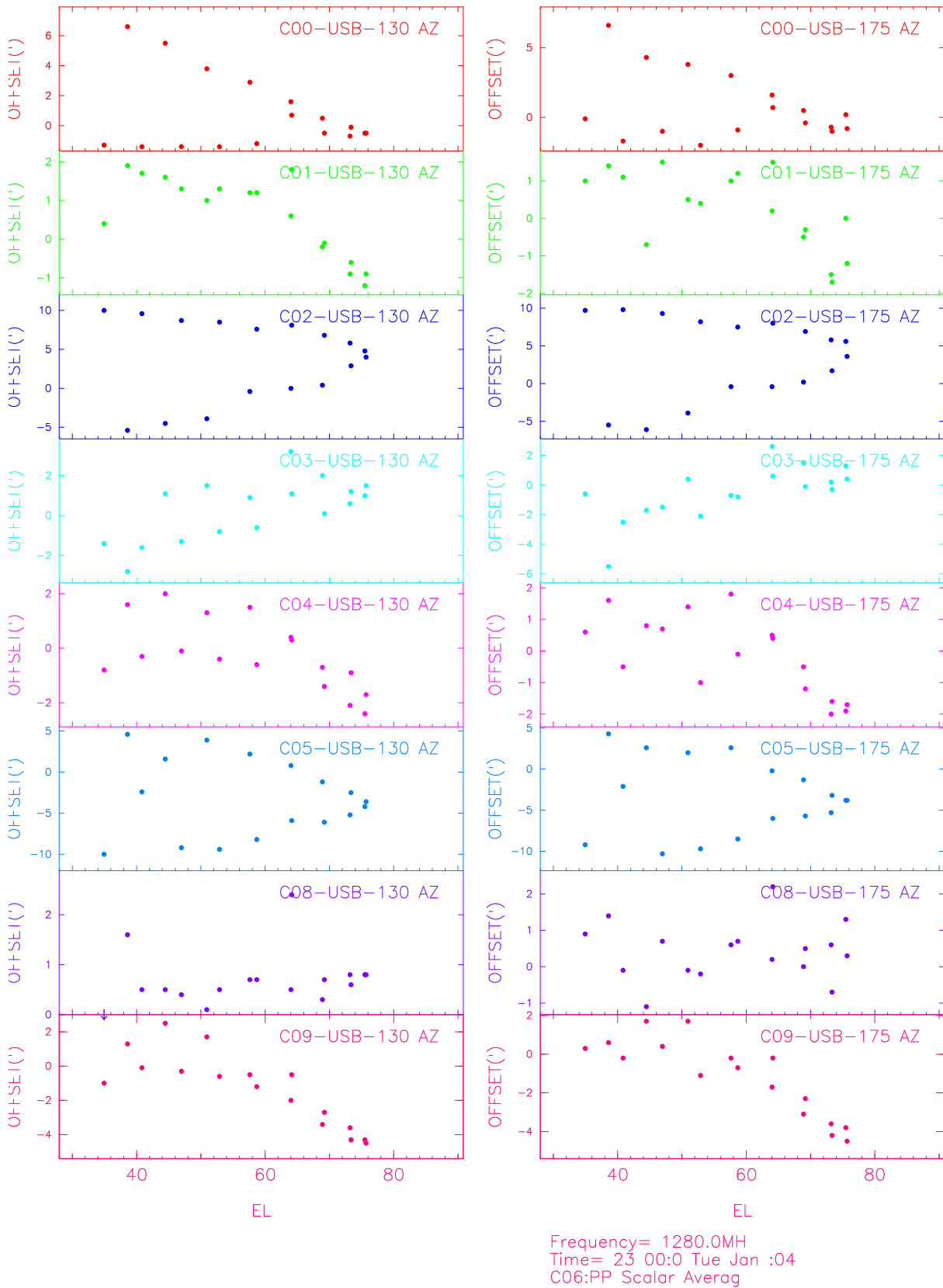


Figure 23: Online application of pointing model on data of 23 January 2007 at 1280 MHz. Plotted here are the azimuth pointing offsets as a function of elevation. Although the rms variation on the offsets is  $\sim 1'$ , a systematic variation seems to be present within this range.

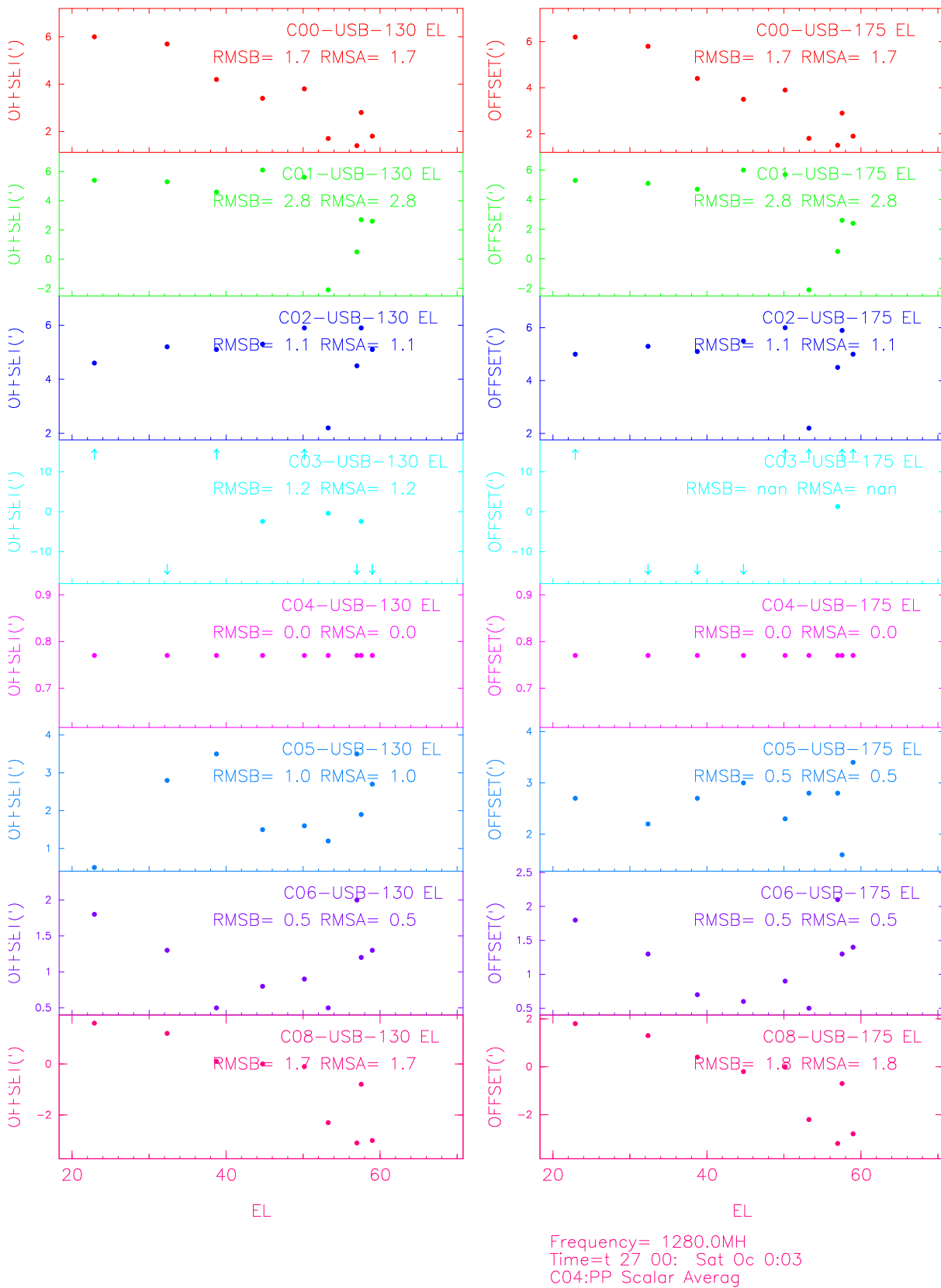


Figure 24: Online application of pointing model on data of 27 October 2007 at 1280 MHz. Plotted here are the elevation pointing offsets as a function of elevation. The RMSB and RMSA are the same since these data have been corrected online. Note that these values for most antennas are  $\leq 1'$  and where its larger, the dominating factor is the hysteresis curve which is evident after the source transits the local meridian

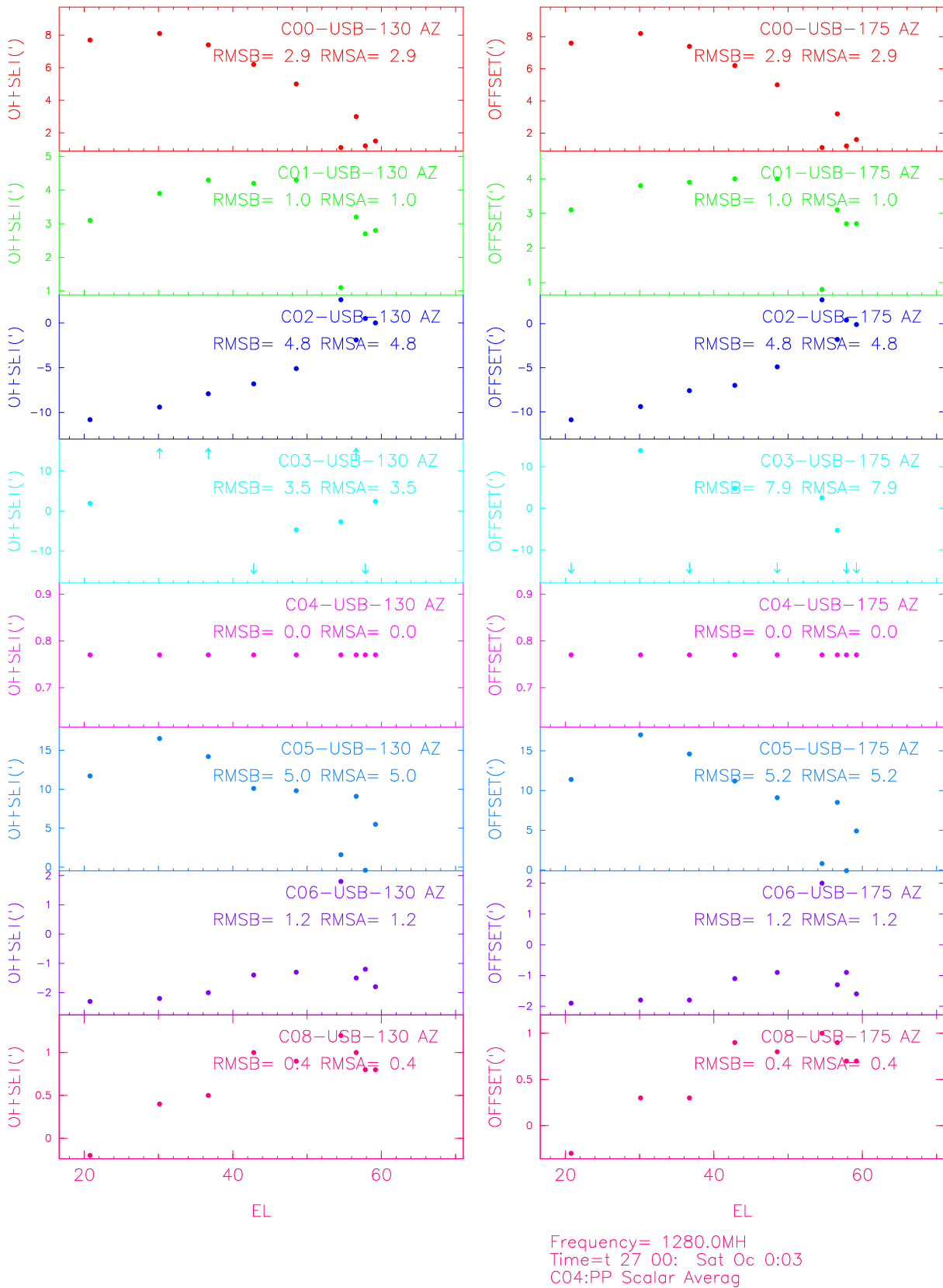


Figure 25: Online application of pointing model on data of 27 October 2007 at 1280 MHz. Plotted here are the azimuth pointing offsets as a function of elevation. Although the rms variation on the offsets is  $\leq 1'$ , a systematic variation seems to be present within this range.

pointing model. The systematic variation in the elevation offsets seen in the uncorrected data in earlier datasets is not present here but the hysteresis persists. The worst cases of hysteresis are C01, E02 and S04. However there does not seem to be any improvement in the azimuth offsets. In fact, a large systematic variation in the azimuth offsets is evident in the plots for most of the antennas inspite of an online correction. This suggests that the pointing model obtained from October 2006 data is no longer applicable to the azimuth pointing offsets and needs to be updated. Figs. 24, 25 shows a similar pair of plots from data obtained on 27 October 2007. Although the data density is low making it difficult to draw firm conclusions, the RMSA and RMSB (both are same in this case since the offsets have been corrected online) for the elevation offsets (Fig. 24) hover around 1' for many of the antennas and this might indicate that the model corrections found elevation offsets in October 2006 might be working. However we believe that this needs to be confirmed. We do not notice any improvement in the variation in azimuth offsets - in fact, the model appears to increase the variation in this data, confirming what we suspected in January 2007 that the model needs to be updated.

## 7 Future work

In this section we suggest some future work to improve and study the time evolution of the pointing model.

- Resolve the problems with the procedure *gopntg*: (1) it should be possible to run it within a command file environment (2) it should be possible to abort the procedure without pushing ONLINE in an indeterminate state (3) reduce the overhead times e.g. for observing nine grid points of elevation and azimuth for a minute each, the procedure takes 30 minutes to run which means the overhead time is 40%. If this is reduced more time can be used to get pointing data.
- Obtain a pointing model from fresh data every six months. Compare coefficients and study the time variation, if any. This will be particularly useful to pinpoint the coefficients which vary with time. From our results, it does appear that the coefficients which describe gravitational deformation and are the major contributors to the variation in the elevation pointing offsets do not change over a long time scale ( $\geq 6$  months). However, the azimuth encoder offset and the inclination of the elevation axis which dominate the variation in the azimuth pointing do change over a shorter time scale ( $\leq 6$  months). TEMPoral monitoring of the model will help determine the differential changes in the coefficients and arrive at an optimum period when the pointing model should be upgraded at GMRT.
- Include the effect of hysteresis in the model where the same elevation gives two different values of the pointing offset depending on whether the data has been taken before or after transit of the object. Since most antennas show hysteresis, noticeable in the form of a jump at 0h HA and a different path henceforth, it would be useful to include this in the model.

- Understanding the peculiar behaviour exhibited by C01 (large range in the variation of elevation pointing offsets), C02 (large peculiar variation in the azimuth pointing offsets), E02 (large jump at 0h HA). Can this be translated to problems in the hardware and communicated to the engineering team?
- Make images of the same region of sky at 1280 MHz: 1) before applying pointing model 2) after applying online pointing model. Compare dynamic range of the two images.

## 8 Summary and Conclusions

Rise-to-set data on four different sources were obtained from 7 to 9 October 2006. The tracks of six sources which had been selected for this experiment in the elevation-azimuth plane are shown in Fig 1b. Due to several system problems, we could only obtain data on four sources. These data were then used to obtain a pointing model for the working antennas less the reference antennas which were kept as C00 and C05. We still don't have a pointing model for these two antennas but we plan to rectify that as soon as the exercise of incorporating the model for rest of the antennas succeeds.

This data was then used and a pointing model obtained for all the antennas. This pointing model was then applied to all the data taken between 7 and 9 October and also data taken on other days (24 August 2006, 6 December 2006, 23 January 2007, 27 October 2007) to check whether the model applies. The results, we obtained, were very encouraging. The pointing model worked well on all the elevation offset data, reducing the rms variation in the elevation pointing offsets for most antennas. Since the rms variation on the azimuth pointing offsets were small to begin with, the results were not so spectacular there. Moreover we think that the model does not work on the 23 January 2007 and the 27 October 2007 data ie the model needs to be updated especially for the azimuth pointing offsets.

Final work on the pointing model is in progress as this report is being written. The report under preparation by Subhashis Roy has more details. The details of the analysis programmes used to analyse the data and generate a pointing model can be found in the report under preparation by Vasant K. Kulkarni.

## 9 Acknowledgements

We thank A. Pramesh Rao for suggesting and implementing some of the options required for efficient pointing observations. We are grateful to the telescope operators, in particular, Santaji, Jitendra, Manish and Deepak for helping beyond duty in the pointing experiment. We thank Yashwant Gupta for several discussions and suggestions. We thank Subhashis Roy for allowing us to modify his script for updating the pointing offsets file. NGK thanks Ravi Subrahmanyam and Miller Goss for information on how pointing is done at ATNF and VLA respectively and Nimesh Patel and

T.K.Sridharan for discussions on the SMA pointing. We are grateful to Dave Green and Tim Garn for useful discussions on pointing and sharing the results they obtained from their own pointing tests at GMRT.

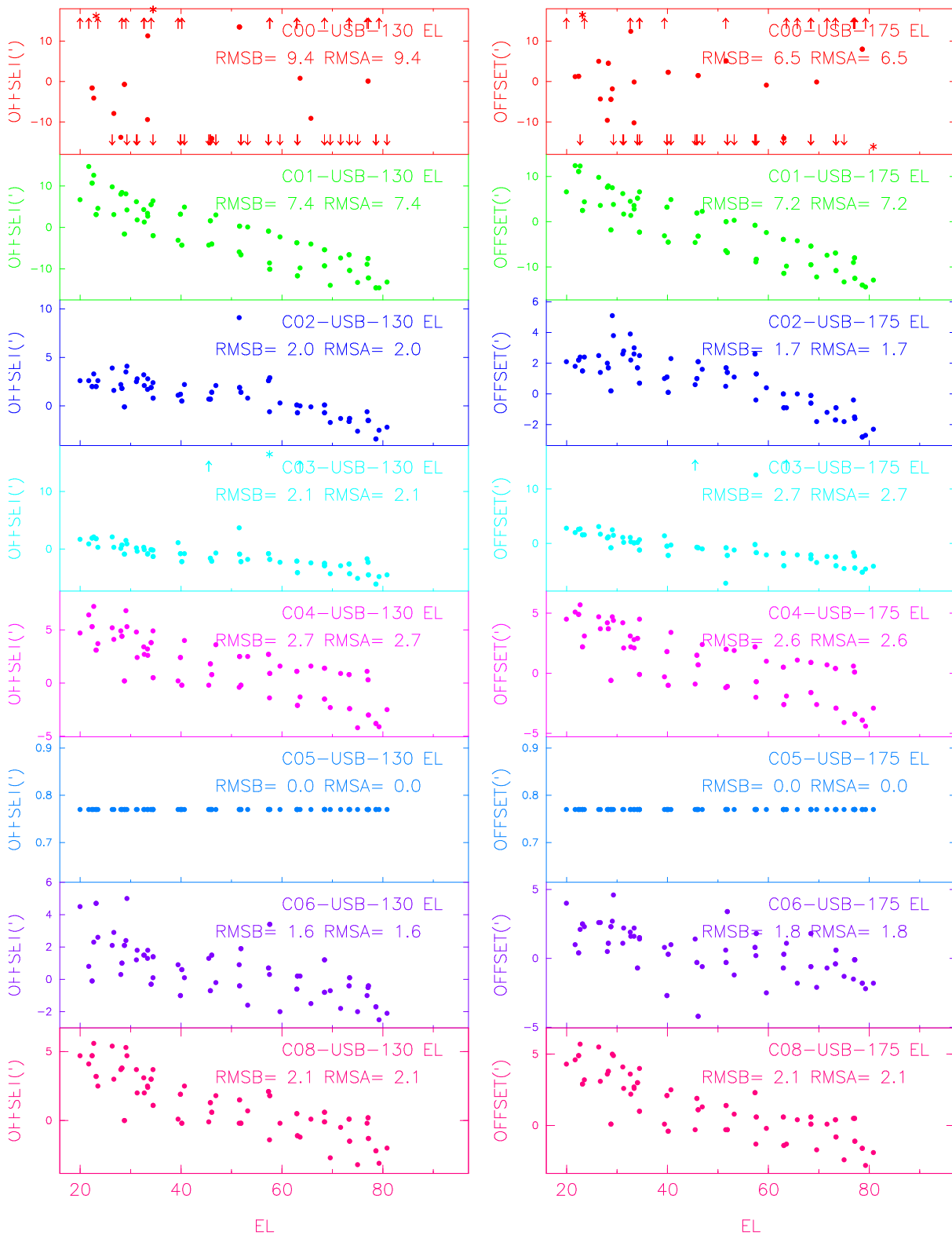
## 10 References

1. Greve, A., Panis, J. -F., Thum, C., ' The pointing of the IRAM 30-m telescope', 1996, A&A Supp Ser. 115, 379.
2. Ulich, B. I., 'Millimeter Wave Radio Telescopes: Gain and Pointing Characteristics' 1981, 2, 293
3. Meeks, M. L., Ball, J. A., Hull, A. B., 'The Pointing Calibration of the Haystack Antenna', IEEE Transactions on Antennas and Propagation, 1968, AP-16, 746
4. Stumpff, P., 1972, Kleinheubacher Berichte, 15, 431
5. Garn, T. 2006, 'Corrections to the GMRT primary beam for observations of the Spitzer extragalactic First Look Survey', Internal report
6. Patel, N., Sridharan, T. K., SPIE, 2008

## 11 Appendix - Pre and Post Pointing model data for all antennas taken between 7 and 9 October 2006

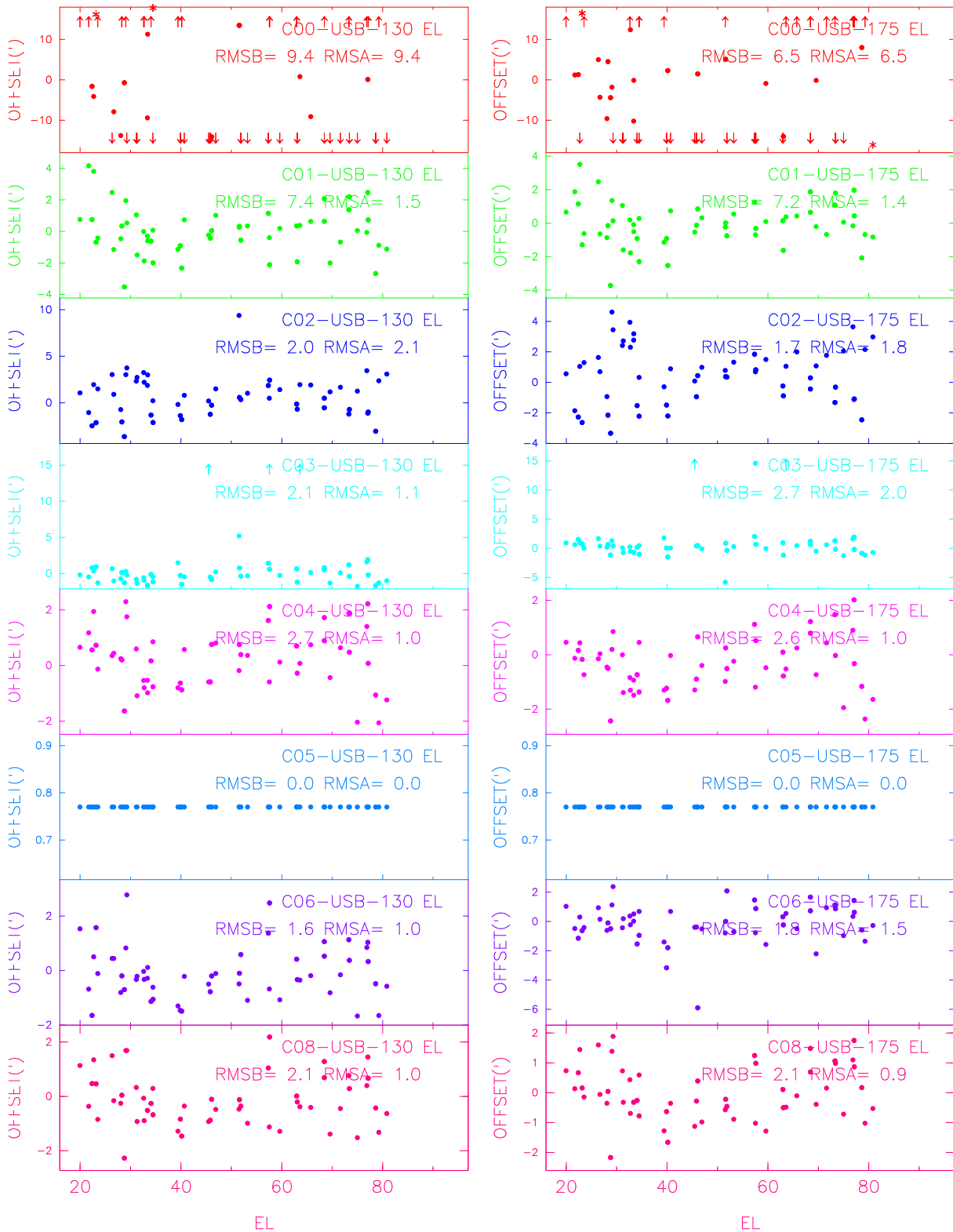
### 11.1 Before applying pointing model

Data on four sources were obtained by observing a grid of points alternately along the elevation and azimuth axes. The plots here show the variation in the pointing offsets along the elevation axis when labelled 'EL' in the top right corner and along the azimuth axis when labelled with 'AZ' in the top right corner.



Frequency= 1280.0MH  
Time= Oct 7 BS= Sat 0:00  
C05:PP Scalar Averag

Figure 26: The elevation pointing offsets determined from several sets of data are plotted as a function of the elevation of the source for 8 antennas. The data were obtained over 7-9 October 2006. No pointing model has been applied to the data. COO and C05 were used as the reference antennas.



Frequency= 1280.0MH  
Time= Oct 7 BS= Sat 0:00  
C05:PP Scalar Averag

Figure 27: The elevation pointing offsets determined from several sets of data are plotted as a function of the elevation of the source for the first 8 antennas. The data were obtained over 7-9 October 2006. Pointing model has been applied to the data. C00 and C05 were used as the reference antennas.

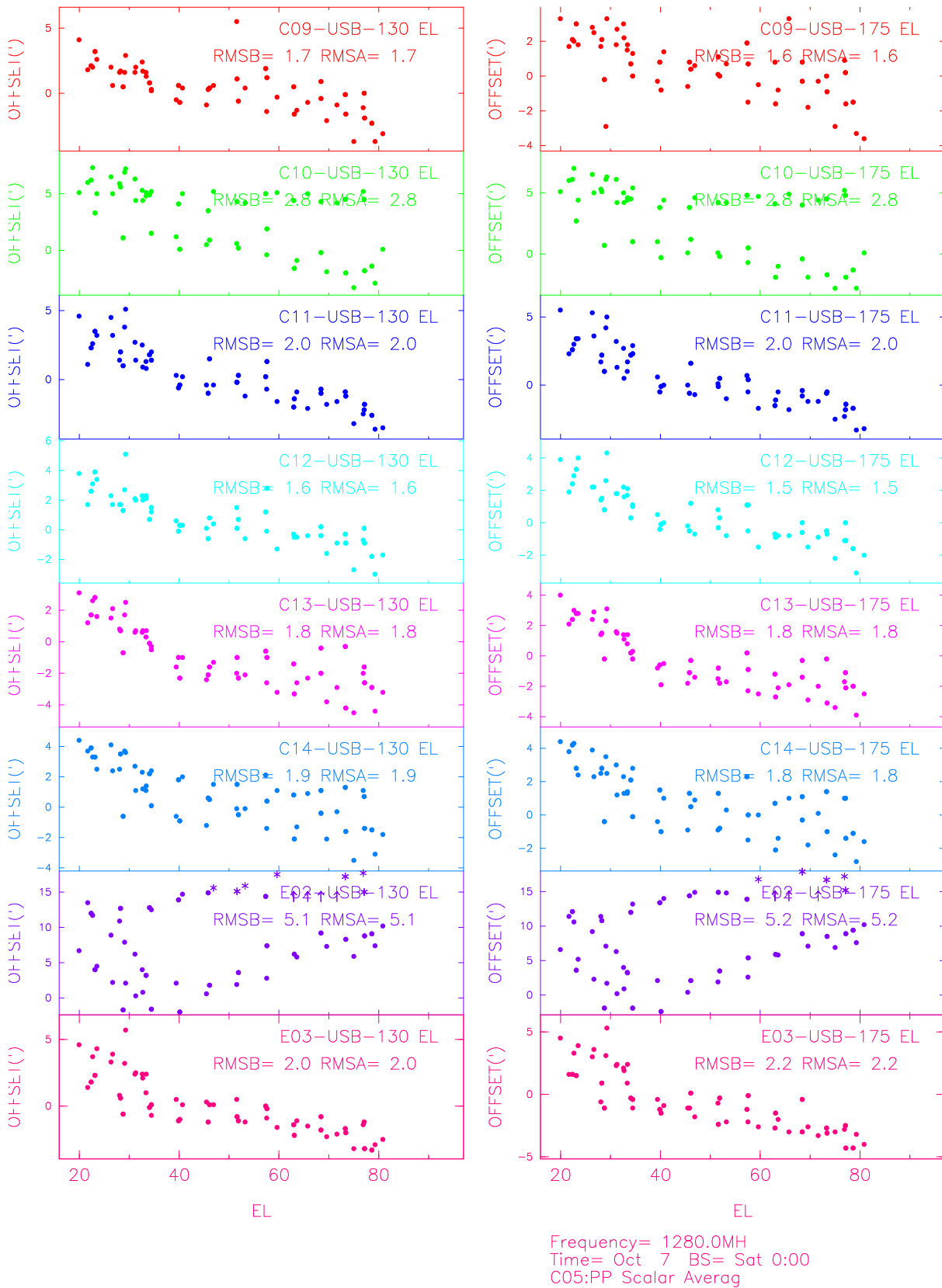


Figure 28: The elevation pointing offsets determined from several sets of data are plotted as a function of the elevation of the source for the next 8 antennas. The data were obtained over 7-9 October 2006. No pointing model has been applied to the data. COO and C05 were used as the reference antennas.

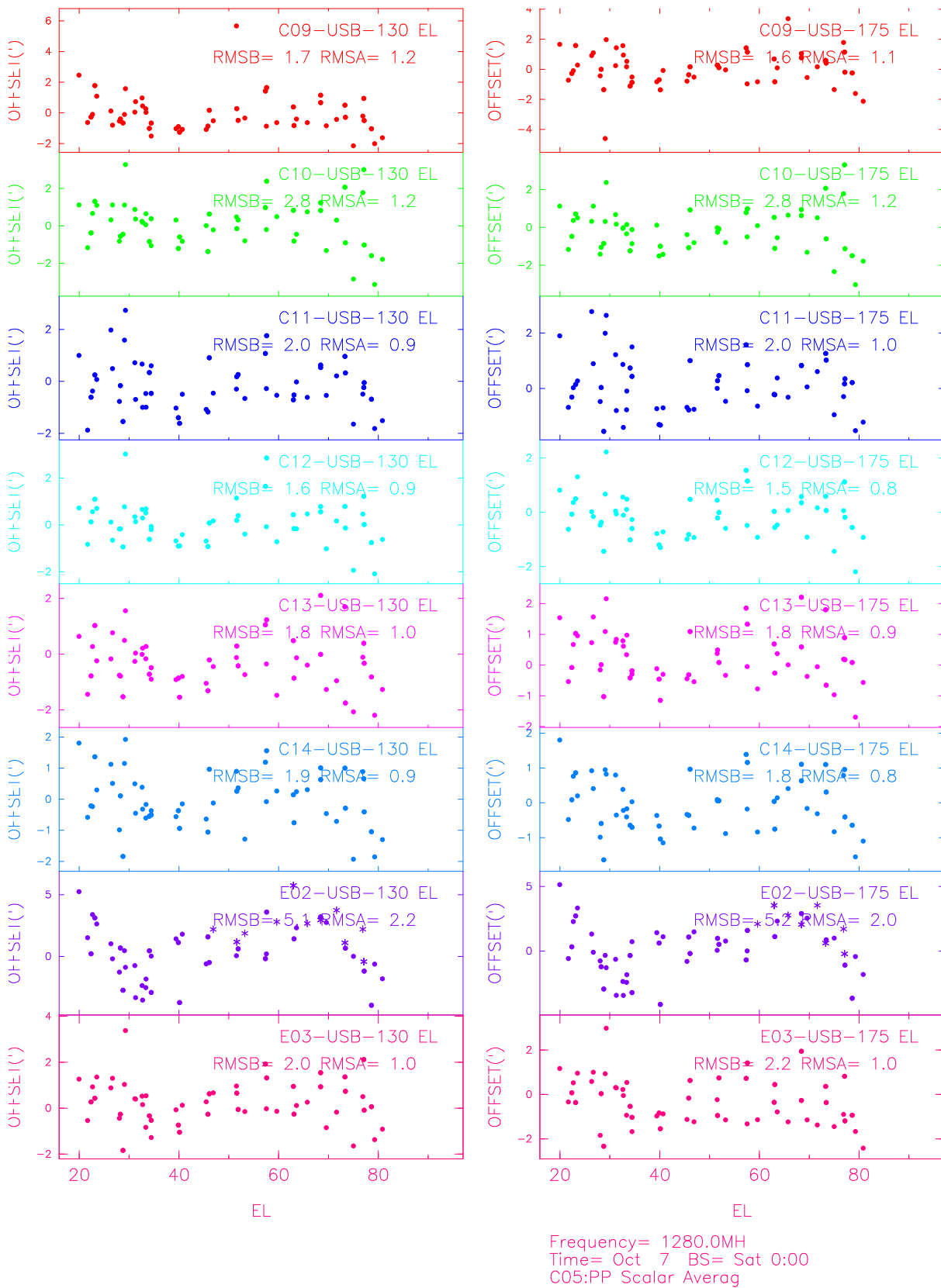


Figure 29: The elevation pointing offsets determined from several sets of data are plotted as a function of the elevation of the source for the next 8 antennas. The data were obtained over 7-9 October 2006. Pointing model has been applied to the data. COO and C05 were used as the reference antennas.

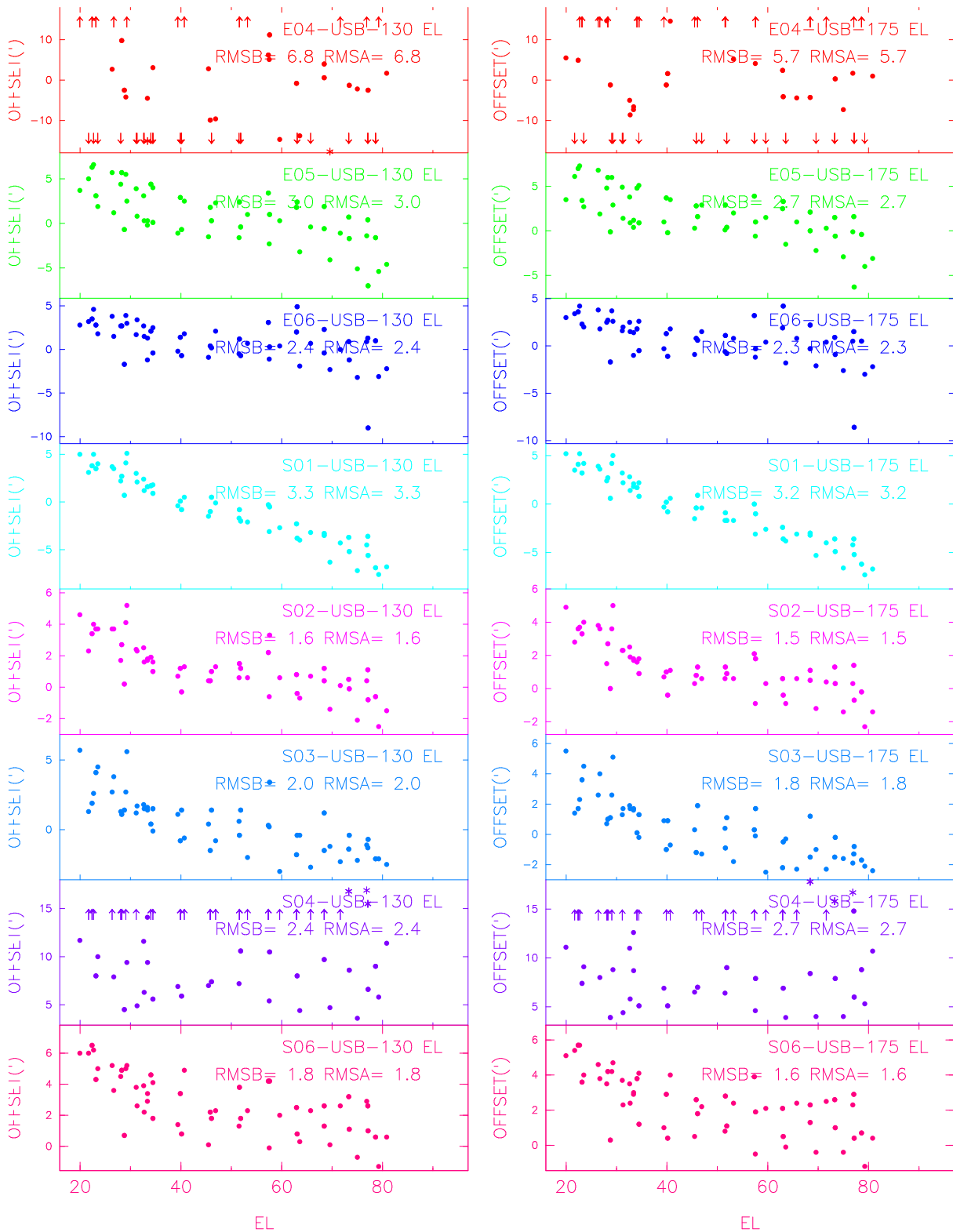


Figure 30: The elevation pointing offsets determined from several sets of data are plotted as a function of the elevation of the source for the next 8 antennas. The data were obtained over 7-9 October 2006. No pointing model has been applied to the data. COO and C05 were used as the reference antennas.

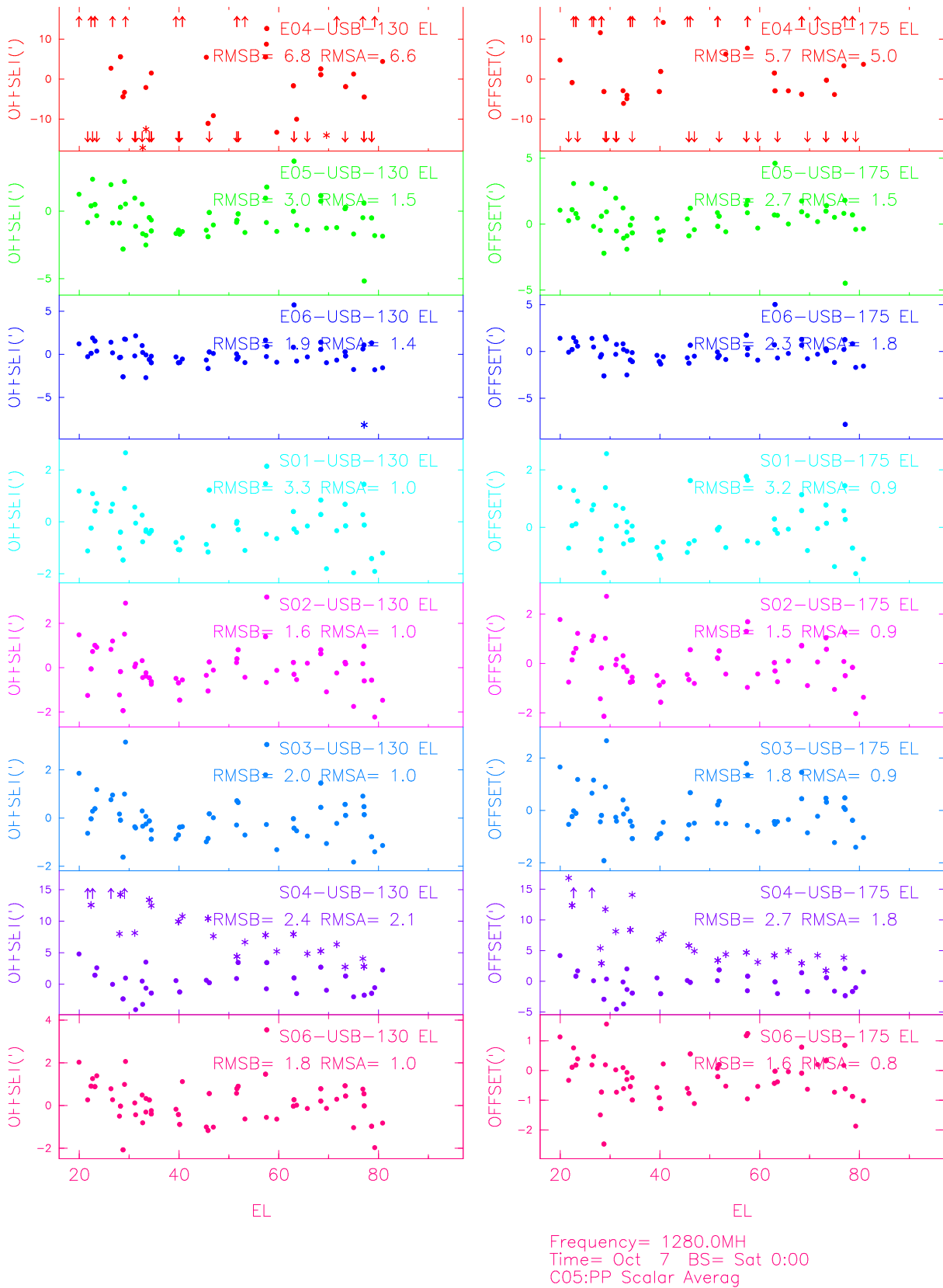


Figure 31: The elevation pointing offsets determined from several sets of data are plotted as a function of the elevation of the source for the next 8 antennas. The data were obtained over 7-9 October 2006. Pointing model has been applied to the data. COO and C05 were used as the reference antennas.

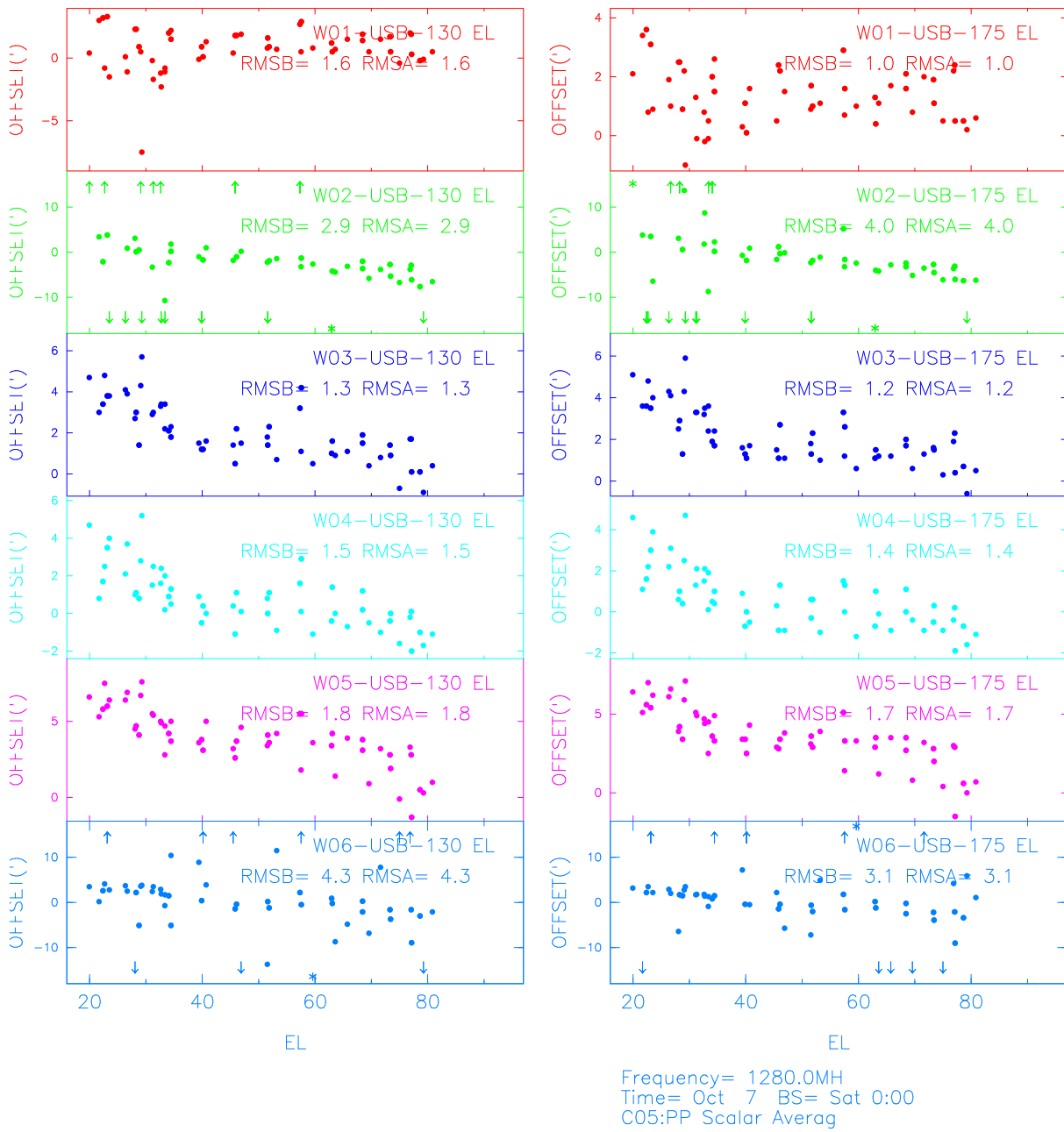


Figure 32: The elevation pointing offsets determined from several sets of data are plotted as a function of the elevation of the source for the last 6 antennas. The data were obtained over 7-9 October 2006. No pointing model has been applied to the data. COO and C05 were used as the reference antennas.

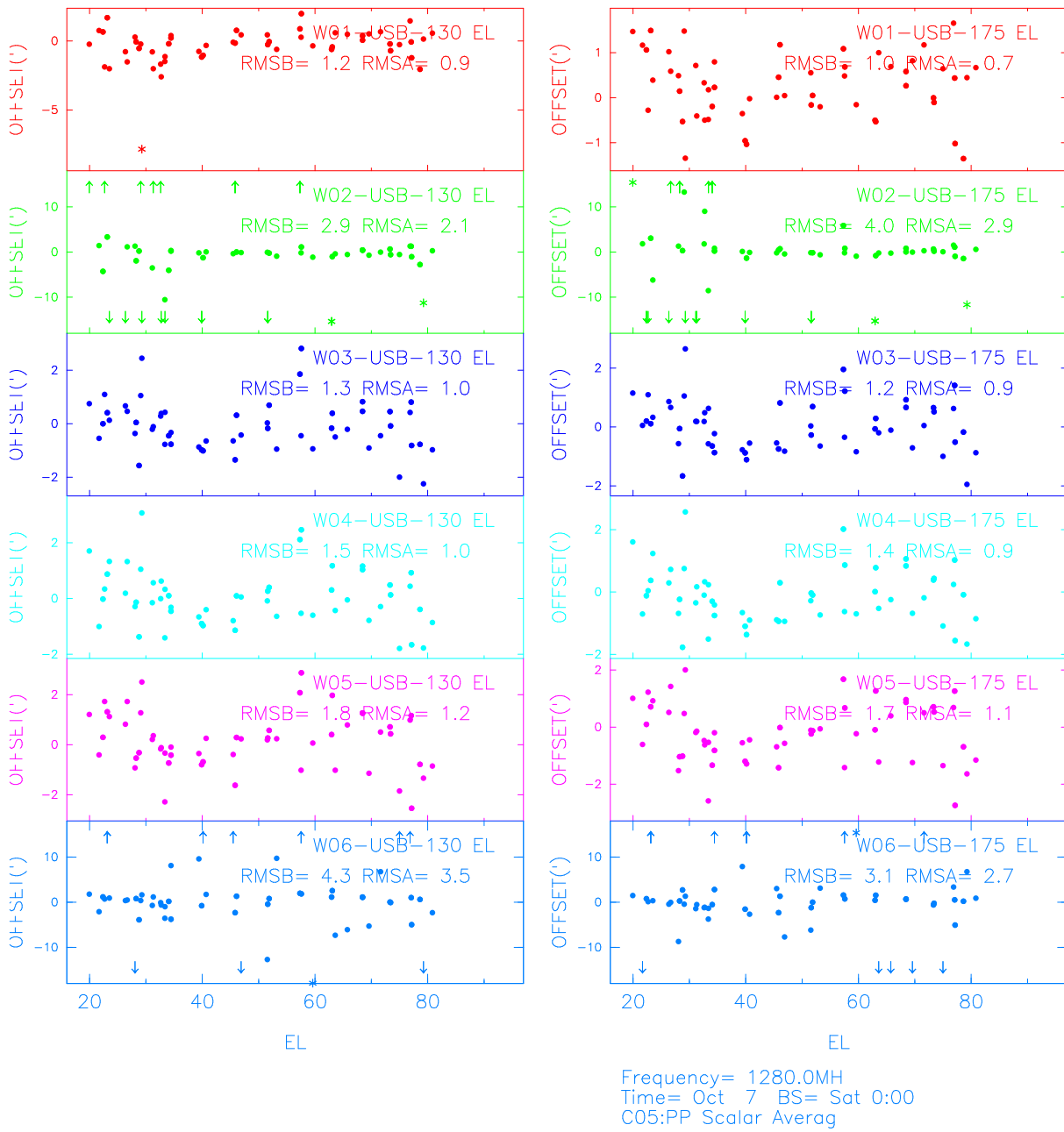


Figure 33: The elevation pointing offsets determined from several sets of data are plotted as a function of the elevation of the source for the last 6 antennas. The data were obtained over 7-9 October 2006. Pointing model has been applied to the data. COO and C05 were used as the reference antennas.

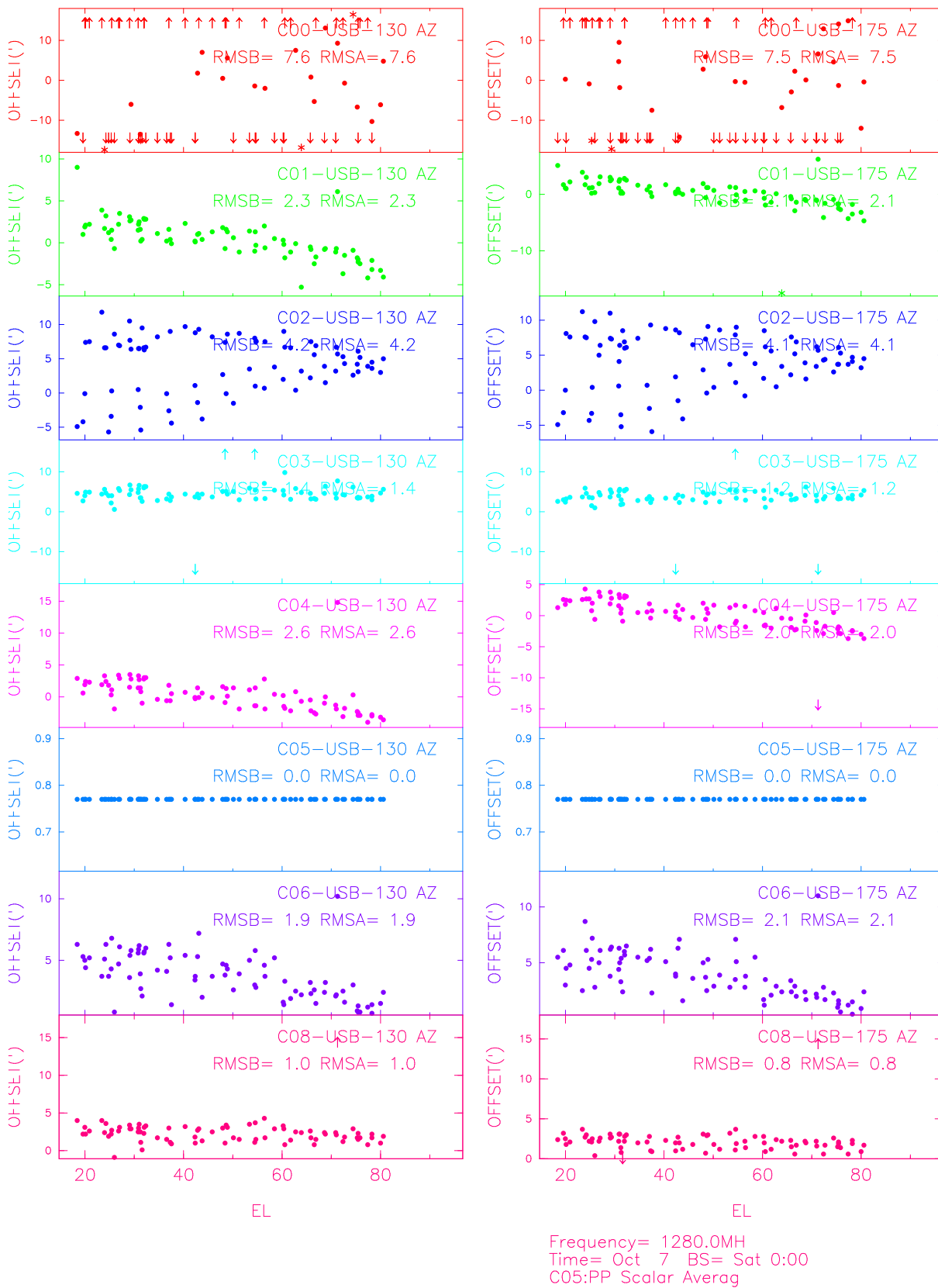
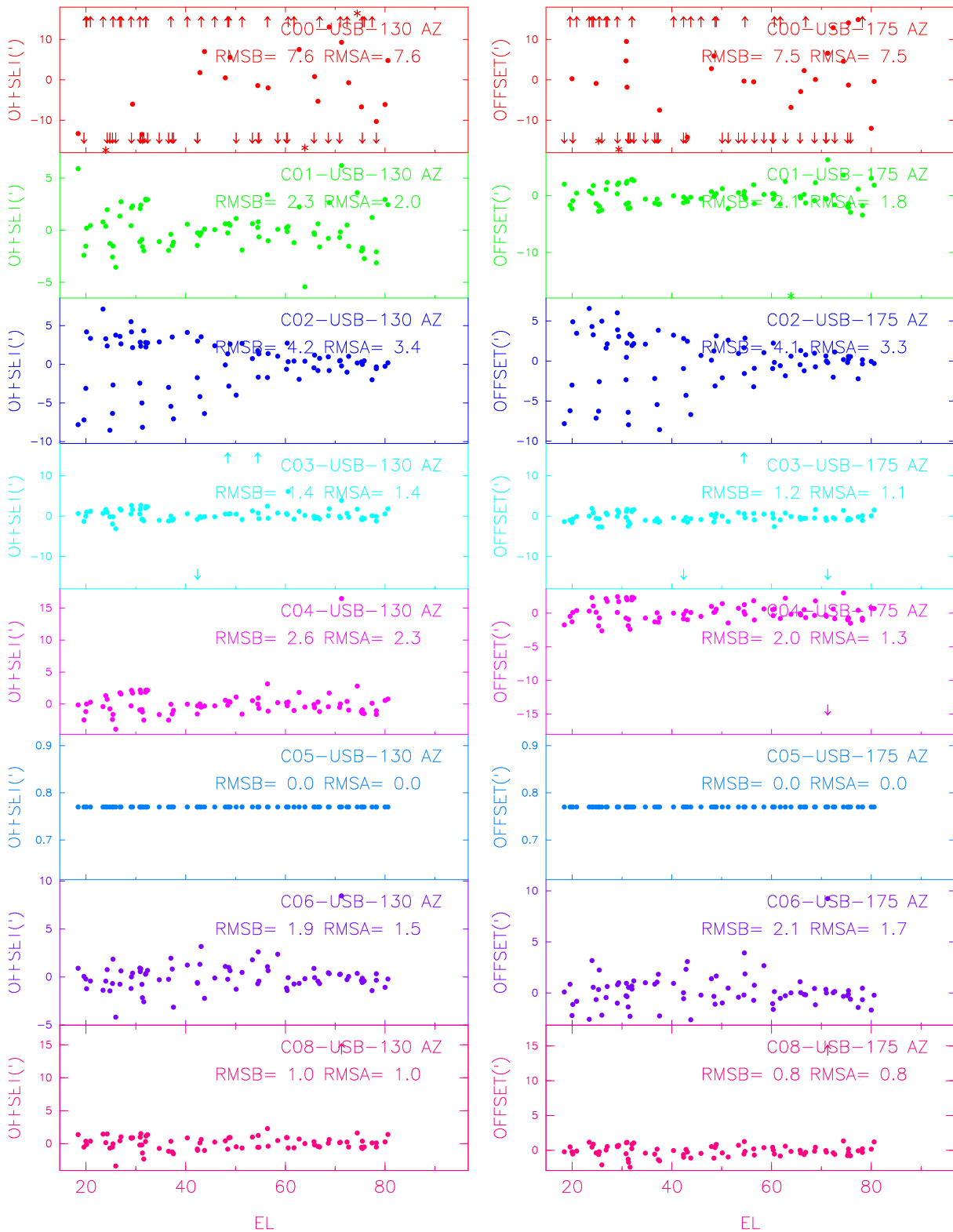


Figure 34: The azimuth pointing offsets determined from several sets of data are plotted as a function of the elevation of the source for the first 8 antennas. The data were obtained over 7-9 October 2006. Pointing model has not been applied to the data. COO and C05 were used as the reference antennas.



Frequency= 1280.0MH  
 Time= Oct 7 BS= Sat 0:00  
 C05:PP Scalar Averag

Figure 35: The azimuth pointing offsets determined from several sets of data are plotted as a function of the elevation of the source for the first 8 antennas. The data were obtained over 7-9 October 2006. Pointing model has been applied to the data. C00 and C05 were used as the reference antennas.

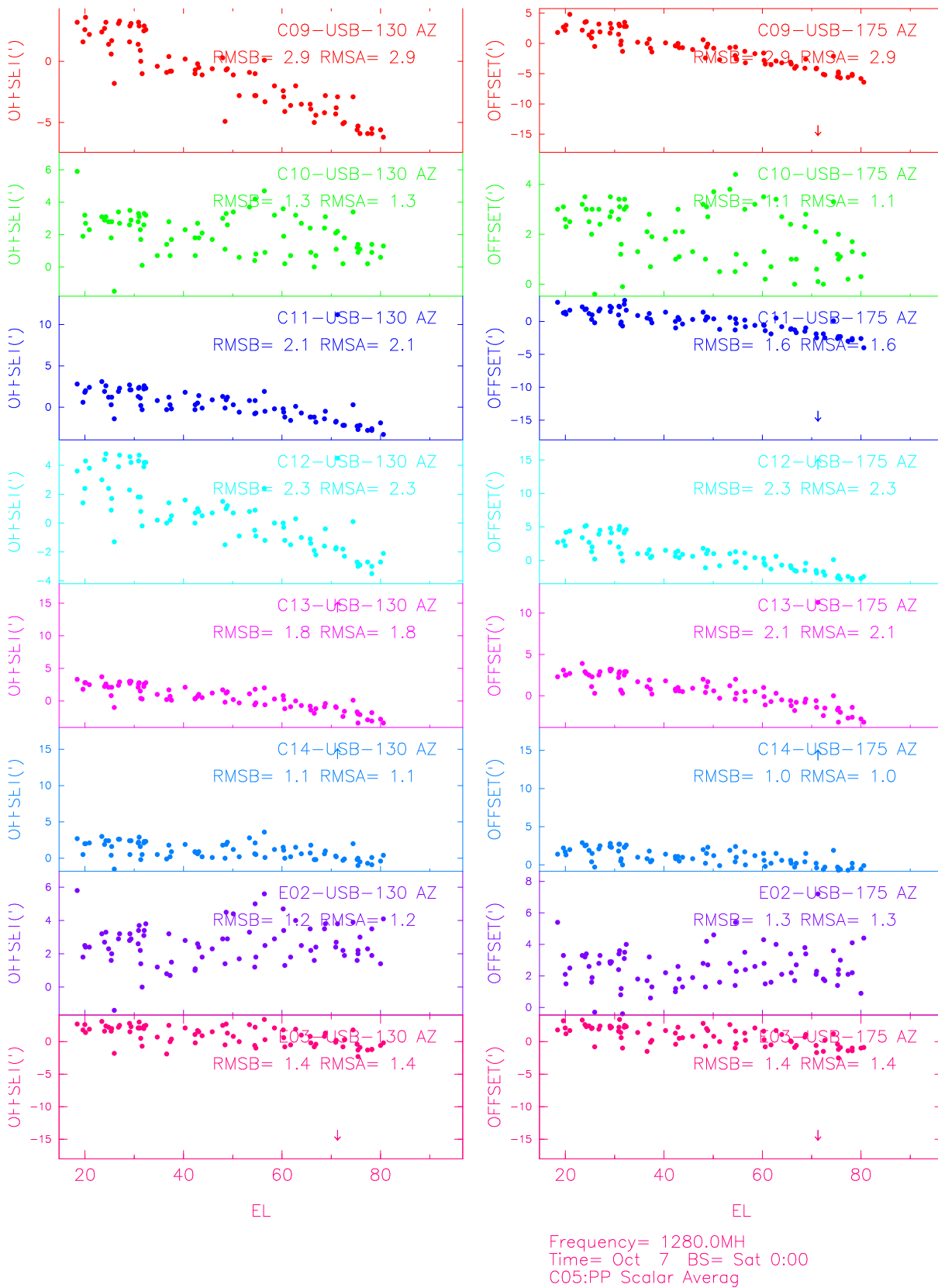
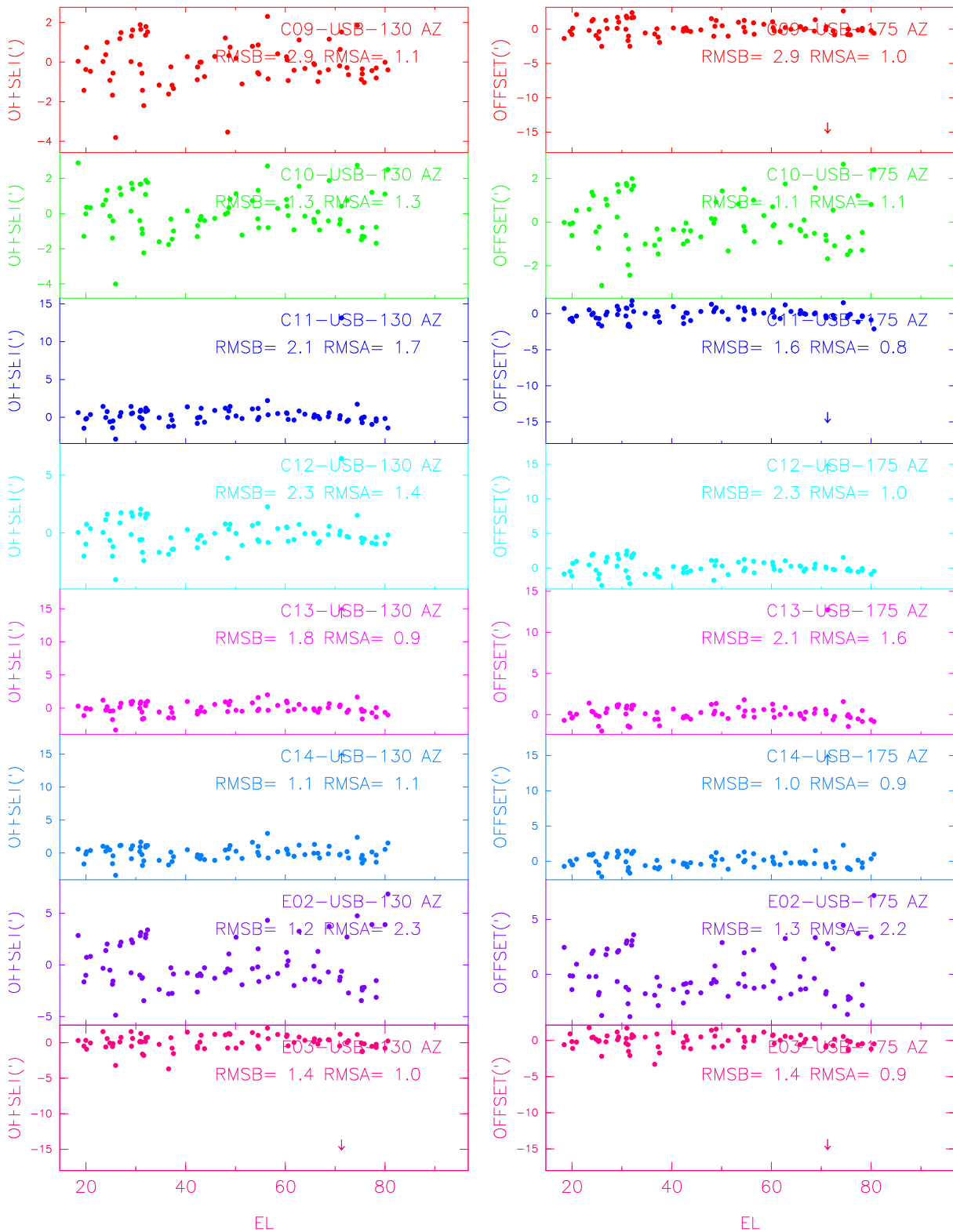


Figure 36: The azimuth pointing offsets determined from several sets of data are plotted as a function of the elevation of the source for the next 8 antennas. The data were obtained over 7-9 October 2006. Pointing model has not been applied to the data. COO and C05 were used as the reference antennas.



Frequency= 1280.0MH  
 Time= Oct 7 BS= Sat 0:00  
 C05:PP Scalar Averag

Figure 37: The azimuth pointing offsets determined from several sets of data are plotted as a function of the elevation of the source for the same 8 antennas shown in the previous figure. The data were obtained over 7-9 October 2006. Pointing model has been applied to the data. C00 and C05 were used as the reference antennas.

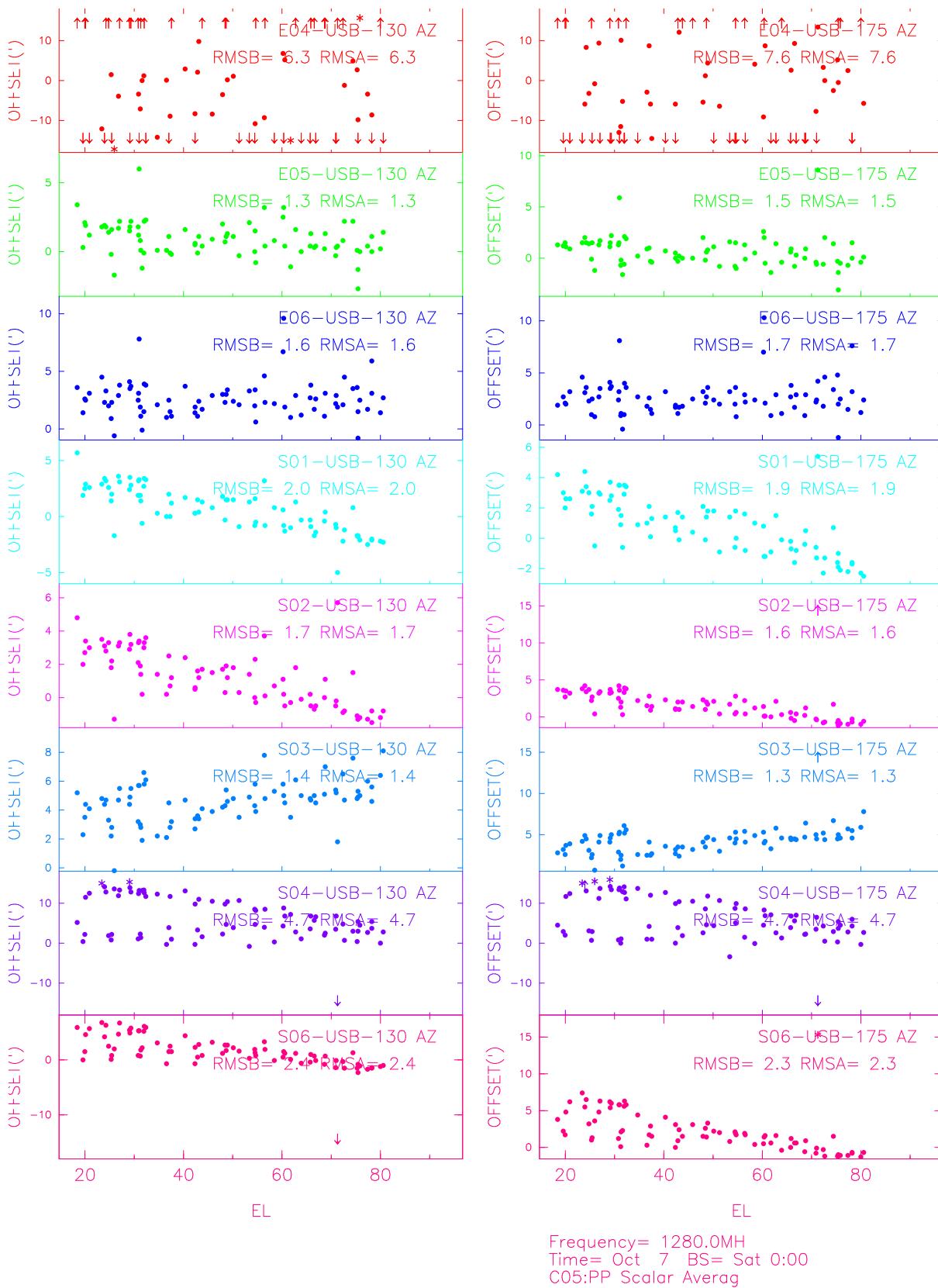
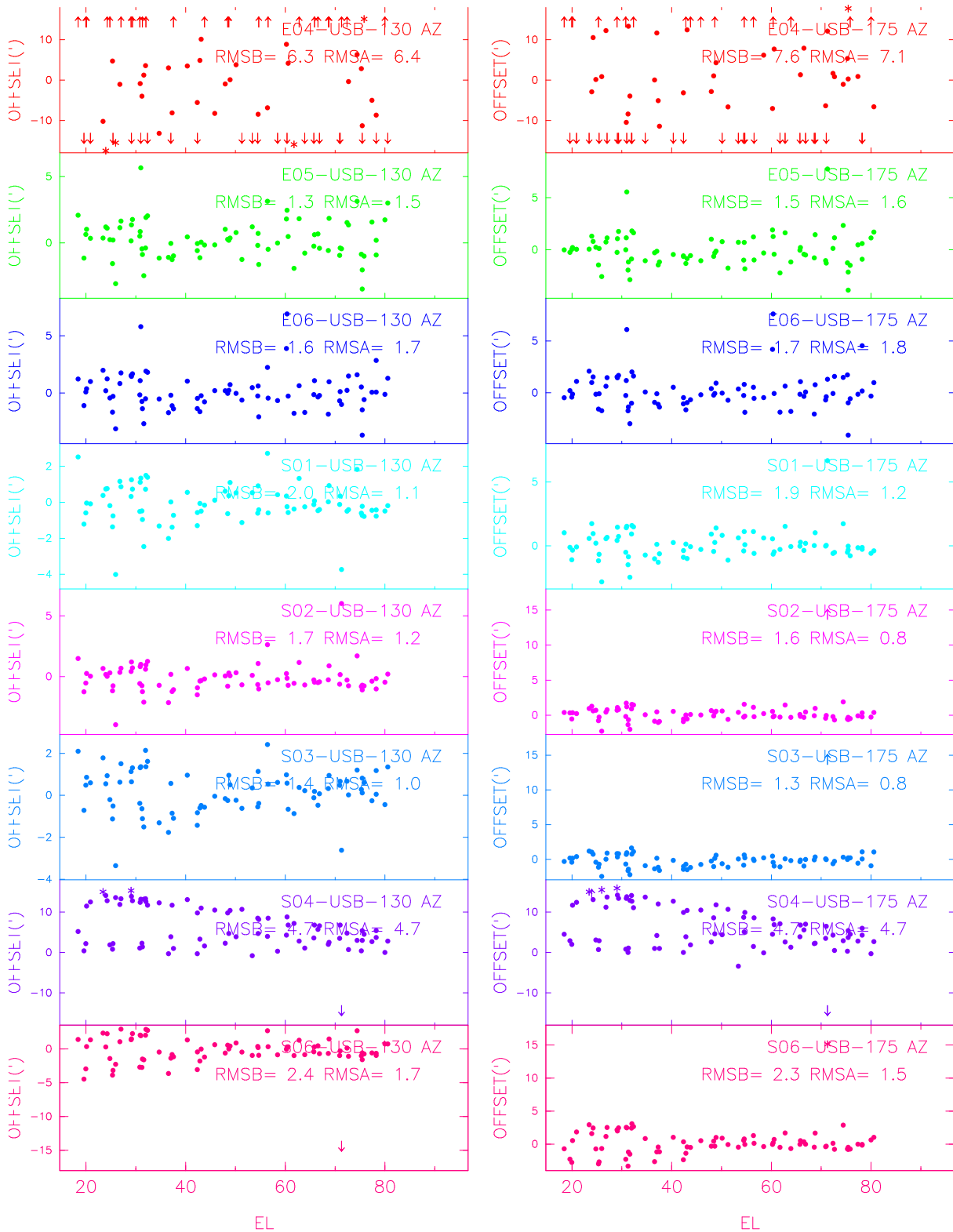


Figure 38: The azimuth pointing offsets determined from several sets of data are plotted as a function of the elevation of the source for the next 8 antennas. The data were obtained over 7-9 October 2006. Pointing model has not been applied to the data. COO and C05 were used as the reference antennas.



Frequency= 1280.0MH  
Time= Oct 7 BS= Sat 0:00  
C05:PP Scalar Averag

Figure 39: The azimuth pointing offsets determined from several sets of data are plotted as a function of the elevation of the source for the same 8 antennas shown in the previous figure. The data were obtained over 7-9 October 2006. Pointing model has been applied to the data. COO and C05 were used as the reference antennas.

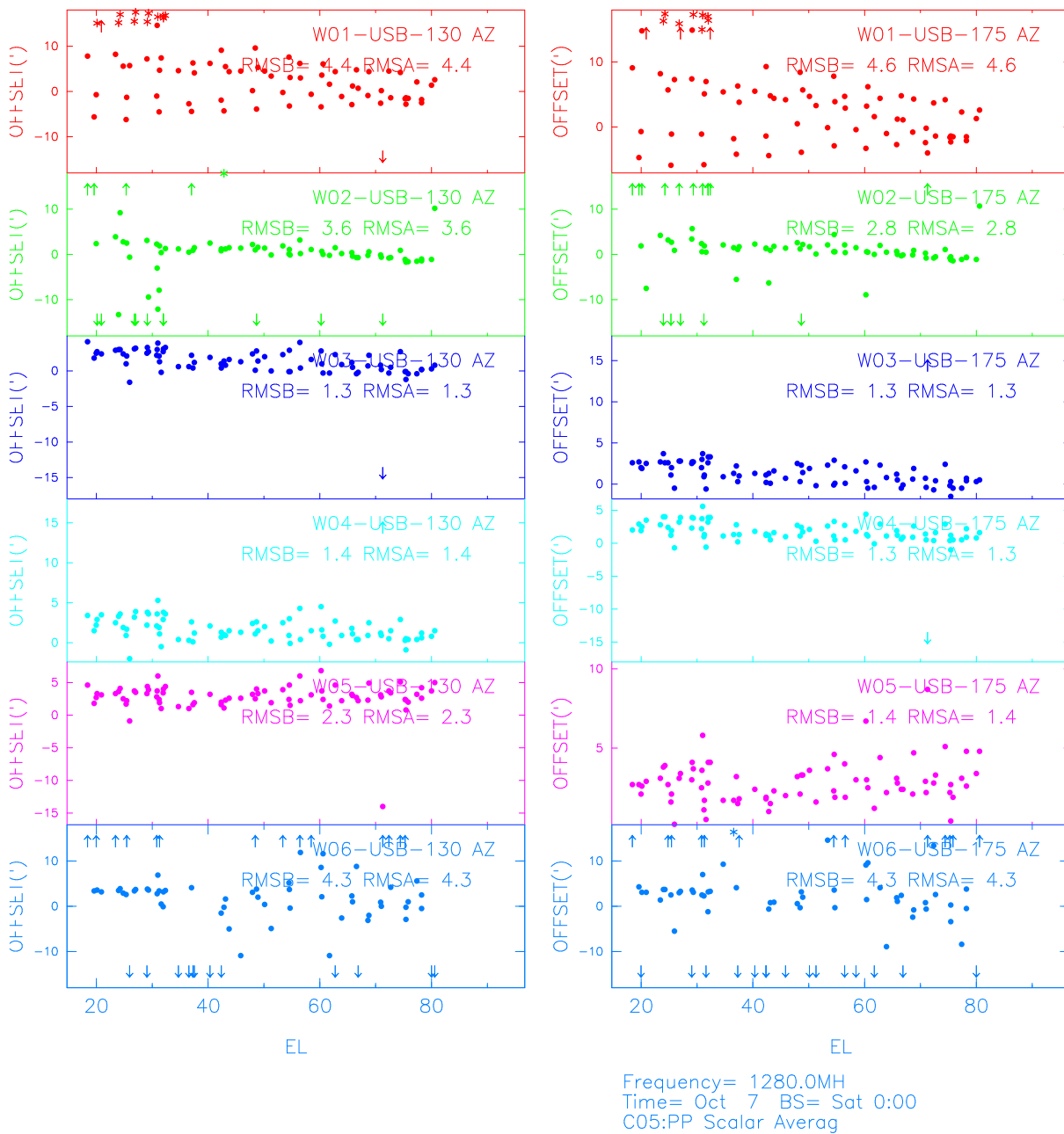


Figure 40: The azimuth pointing offsets determined from several sets of data are plotted as a function of the elevation of the source for the last 6 antennas. The data were obtained over 7-9 October 2006. Pointing model has not been applied to the data. COO and C05 were used as the reference antennas.

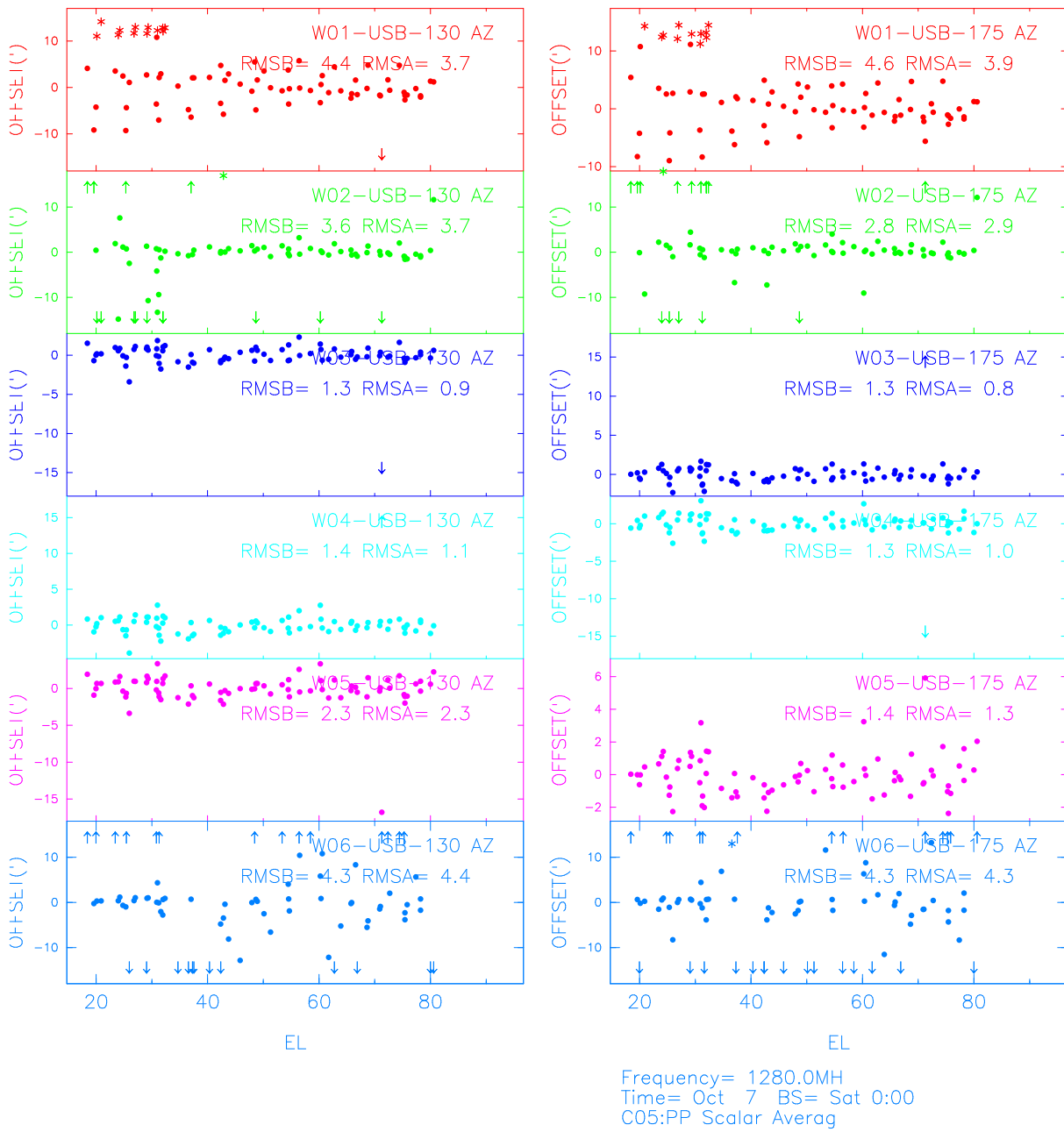


Figure 41: The azimuth pointing offsets determined from several sets of data are plotted as a function of the elevation of the source for the same 6 antennas shown in the previous figure. The data were obtained over 7-9 October 2006. Pointing model has been applied to the data. C00 and C05 were used as the reference antennas.